nature cardiovascular research

Article

https://doi.org/10.1038/s44161-025-00752-9

Rapid mitochondrial repolarization upon reperfusion after cardiac ischemia

Received: 17 December 2024

Accepted: 28 October 2025

Published online: 11 December 2025

Check for updates

Abigail V. Giles[1,2], Raul Covian[1], Hiran A. Prag[3], Nils Burger[2], Bertrand Lucotte[1], Chak Shun Yu[2], Junhui Sun[1], Elizabeth Murphy[1], Thomas Krieg[3], Michael P. Murphy[2,3] ✉ & Robert S. Balaban[1] ✉

The mitochondrial membrane potential ($\Delta\Psi_m$) drives oxidative phosphorylation and alterations contribute to cardiac pathologies, but real-time assessment of $\Delta\Psi_m$ has not been possible. Here we describe noninvasive measurements using mitochondrial heme b_L and b_H absorbances, which rapidly respond to $\Delta\Psi_m$. Multi-wavelength absorbance spectroscopy enabled their continuous monitoring in isolated mitochondria and the perfused heart. Calibration of heme *b* absorbance in isolated mitochondria revealed that reduced heme b_L relative to total reduced heme *b* ($fb_L = b_L/(b_L + b_H)$) exhibits a sigmoidal relationship with $\Delta\Psi_m$. Extrapolating this relationship to the heart enabled estimation of $\Delta\Psi_m$ as 166 ± 18 mV ($n = 25$, mean ± s.d.). We used this approach to assess how $\Delta\Psi_m$ changes during ischemia–reperfusion injury, an unknown limiting the understanding of ischemia–reperfusion injury. In perfused hearts, $\Delta\Psi_m$ declined during ischemia and rapidly reestablished upon reperfusion, supported by oxidation of the succinate accumulated during ischemia. These findings expand our understanding of ischemia–reperfusion injury.

During mitochondrial oxidative phosphorylation (Fig. 1a), the respiratory chain pumps protons across the mitochondrial inner membrane to establish a protonmotive force (Δp), composed of a large electrical potential gradient ($\Delta\Psi$, negative inside) and a smaller pH gradient (ΔpH, basic inside)[1,2]. The Δp drives adenosine triphosphate (ATP) synthesis and export to the cytosol, ion transport, protein import and thermogenesis, as well as the production of superoxide ($O_2^{\bullet-}$), which is the proximal reactive oxygen species (ROS) in many pathologies (Fig. 1b)[2,3]. In the heart, ATP production is largely driven by oxidative phosphorylation[4], but the magnitude of the mitochondrial membrane potential ($\Delta\Psi_m$) (the dominant component of Δp[2]) remains unclear. Furthermore, $\Delta\Psi_m$ is thought to have a key role in several aspects of cardiac ischemia–reperfusion injury including the production of ROS (Fig. 1b)[1,5], the capacity to produce ATP and mitochondrial calcium handling. However, it has not been possible to noninvasively measure $\Delta\Psi_m$ in the intact heart during ischemia–reperfusion injury. To address these critical, unresolved issues, here we quantified rapid changes in $\Delta\Psi_m$ in real time within the isolated perfused mouse heart subjected to global ischemia–reperfusion using endogenous chromophores.

Results

Quantification of $\Delta\Psi_m$ using *b* hemes

Lipophilic cations are accumulated within the mitochondria in response to $\Delta\Psi_m$ and the plasma membrane potential ($\Delta\Psi_p$) in accordance with the Nernst equation and, thus, are commonly used for determining $\Delta\Psi_m$ in vitro[6,7]. Changes in $\Delta\Psi_m$ within cells can be inferred from the distribution of fluorescent lipophilic cations including tetramethylrhodamine methyl ester (TMRM). Ion-selective electrodes can be used to determine $\Delta\Psi_m$ in suspensions of isolated mitochondria incubated with lipophilic cations such as triphenylmethylphosphonium ($TPMP^+$)[8]. Non-optical approaches with potential application in vivo include assessing the distribution of radiolabeled lipophilic cations[9–11] or direct visualization of positron emission tomography tracers incorporated into lipophilic cations[12,13]. Optical approaches for assessing mitochondrial activity that have been applied to the isolated perfused heart

[1]NHLBI, National Institutes of Health, Bethesda, MD, USA. [2]MRC Mitochondrial Biology Unit, University of Cambridge, Cambridge, UK. [3]Department of Medicine, University of Cambridge, Cambridge, UK. ✉e-mail: mpm37@cam.ac.uk; balabanr@nhlbi.nih.gov

https://doi.org/10.1038/s44161-025-00752-9

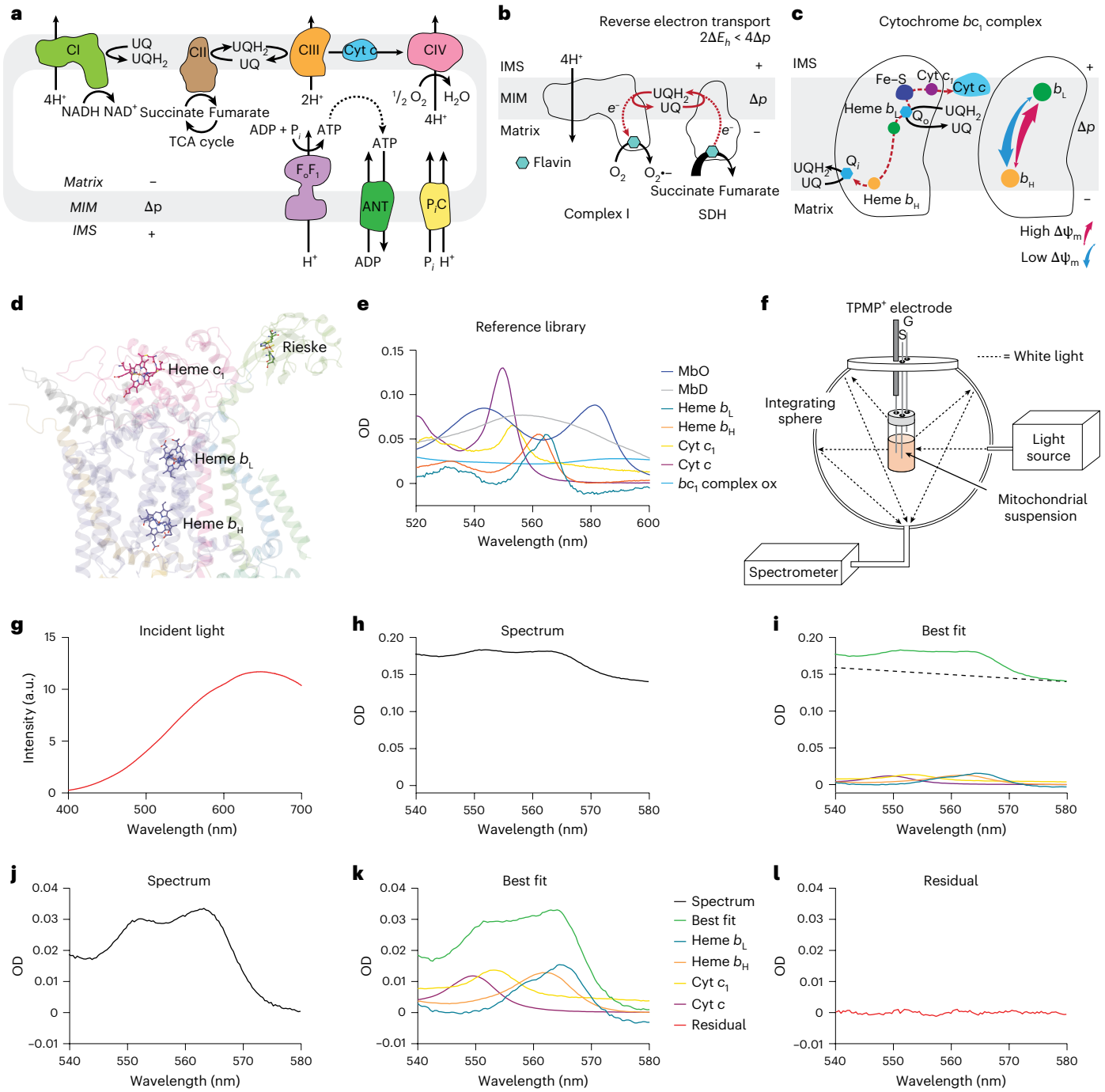

Fig. 1 | Multi-wavelength absorbance spectroscopy in isolated mitochondria. **a**, Mitochondrial oxidative phosphorylation. **b**, Upon reperfusion, succinate accumulated during ischemia is proposed to be oxidized by SDH, driving RET and superoxide production initiating ischemia–reperfusion injury. IMS, intermembrane mitochondrial space; MIM, mitochondrial inner membrane. **c**, Electron transfer within the cytochrome bc_1 complex and electron distribution between hemes b_L and b_H in response to $\Delta\Psi_m$. **d**, Structure of the bovine cytochrome bc_1 complex from PDB 1BE3. The distinct coordination environments of the heme groups in the bc_1 complex give rise to unique absorption spectra. **e**, Reference spectra including for reduced hemes b_L and b_H and cytochromes c_1 and *c* and for oxygenated (MbO) and deoxygenated (MbD) purified mouse myoglobin, as well as oxidized cytochrome bc_1 complex, were collected using a combination of biochemical techniques. Thus, relative optical density (OD) is arbitrary. **f**, Schematic of the integrating sphere system used to measure the optical absorbance of mitochondrial suspensions. $TPMP^+$ distribution was measured simultaneously by a $TPMP^+$-selective electrode. Substrates, inhibitors and uncouplers (S) and gases (G) were introduced via separate ports. **g**, Spectrum of incident light used to analyze mitochondrial suspensions. a.u., arbitrary units. **h**, Isolated mitochondria were incubated with succinate/rotenone, and a multi-wavelength nonlinear least squares regression was performed on the experimental absorbance spectrum using reference spectra for mitochondrial hemes and cytochromes and a line. **i**, The best fit and individual chromophore contributions. **j**,**k**, The linear component, incorporated into the fit to account for absorption by the integrating sphere and oxidized chromophores, was subtracted from the experimental spectrum (**j**) and best fit (**k**). **l**, The residuals of the best fit.

include assessing the redox state of NAD(P)H and flavoprotein pools by autofluorescence[14,15] and monitoring the fluorescence of lipophilic cationic dyes such as safranine[16] or TMRM[17]. However, the application of lipophilic probes and dyes is challenging in the intact, perfused heart due to uncertainty about the uptake, binding and distribution of these probes[18]. Furthermore, using these approaches to quantify $\Delta\Psi_m$ relies on multiple assumptions[8], while the slow equilibration of lipophilic cations within tissues[19] precludes the rapid assessment of $\Delta\Psi_m$ changes that is required to understand how $\Delta\Psi_m$ responds to ischemia–reperfusion injury.

To overcome these limitations, here we quantified $\Delta\Psi_m$ in real time using endogenous chromophores. The mitochondrial cytochrome bc_1 complex contains b_L (lower reduction potential, $E_m = -90$ mV (ref. 20)) and b_H (higher reduction potential, $E_m = -30$ mV (ref. 20)) hemes positioned close to the positive and negative sides of the inner membrane, respectively (Fig. 1c)[21]. During respiration, electrons are reversibly transferred from b_L to b_H, which also exchanges electrons with the coenzyme Q (CoQ) pool. The exchange of electrons between b_L and b_H depends on the relative reduction potential of these hemes and on $\Delta\Psi_m$, with a decrease in $\Delta\Psi_m$ favoring electron migration from b_L to b_H (Fig. 1c). Thus, the amount of reduced b_L relative to reduced b_H provides insight into $\Delta\Psi_m$. The optically distinct absorbance of each *b* heme increases in the reduced state, so as $\Delta\Psi_m$ rises, the absorbance of b_L is expected to increase relative to that of b_H. To compensate for the changes in the redox state of the cytochrome bc_1 complex due solely to differences in respiration rate or substrate availability, the fraction of reduced heme b_L should be normalized to the amount of total reduced *b* heme ($b_L + b_H$). Following this approach, we generated a parameter $fb_L = b_L/(b_L + b_H)$ that is highly sensitive to $\Delta\Psi_m$ and can be calculated from the absorbance of the b_L and b_H hemes. This approach is possible because the distinct coordination environments of the heme groups in the bc_1 complex (Fig. 1d) give rise to unique absorbance spectra, enabling multi-wavelength absorbance spectroscopy. Hemes b_H and b_L are spectrally distinct with absorption peaks at 562 nm and 564 nm, respectively (Fig. 1e). Over the bandwidth of interest where the reduced hemes of the cytochrome bc_1 complex absorb (540–580 nm), there is also absorption by reduced cytochrome *c* and cytochrome c_1 (Fig. 1e). Reduced cytochrome *c* has peak absorption at 550 nm, whereas reduced cytochrome c_1 ($E_m = 230$ mV[22]) is slightly red shifted with peak absorption at 552 nm.

The relationship between b_L/b_H reduction and $\Delta\Psi_m$ was established in submitochondrial particles[23] and cytochrome bc_1 reconstituted into liposomes[24], with this relationship later extrapolated to cultured cells to estimate $\Delta\Psi_m$ (ref. 25). While promising in principle, optical analysis in cells was limited because the calculation of $\Delta\Psi_m$ was inferred from midpoint reduction potential ($E°$) values for the *b* hemes obtained in vitro[26]. Therefore, to use this method to quantify $\Delta\Psi_m$ in the intact, perfused heart from the reduction states of b_L and b_H, fb_L has to be calibrated against an orthogonal measure of $\Delta\Psi_m$, to avoid using $E°$ values generated under nonphysiological conditions.

Calibrating *b* heme absorbance against $\Delta\Psi_m$

While optical methods have been used to study mitochondrial cytochromes for many decades[27,28], quantification of cytochrome reduction status has usually relied on dual-wavelength analysis in which absorbance peaks are measured relative to absorbance minima or putative isosbestic points[29]. However, this approach is unreliable, particularly in complex systems such as the intact heart, due to the overlapping spectral features of biochemically independent chromophores[30–32]. Consequently, dual-wavelength analysis has been superseded by multi-wavelength absorbance spectroscopy and spectral analysis, which has been applied to isolated mitochondria and the perfused heart[30–32]. The advantage of using multi-wavelength spectral fitting is that the spectral density at all wavelengths is used to determine the absorption of individual cytochromes, rather than relying on single peak absorption wavelengths, which greatly facilitates the deconvolution of spectrally similar cytochromes, enabling robust determination of b_L and b_H absorbance. Here, we used multi-wavelength absorbance spectroscopy to determine the reduction state of mitochondrial *b* hemes within both isolated mitochondria and the perfused mouse heart.

To determine the absorbance of b_L and b_H, and thus fb_L, in isolated mitochondria, the optical absorbance of heart mitochondria was determined using an integrating sphere system optimized to capture light scattered by the turbid suspension (Fig. 1f) and then fit with reference spectra for reduced (Fe^{2+}) cytochromes (Fig. 1e). This reference library was generated in the integrating sphere system using a combination of biochemical techniques, which are described in detail in the Methods section. For this reason, the optical density of the reference spectra does not reflect absolute absorption. A white light source (Fig. 1g) was passed through the sample. Experimental absorbance spectra (Fig. 1h) from 540 to 580 nm were fit with reference spectra representing reduced heme b_H, heme b_L, cytochrome c_1 and cytochrome *c* using a nonlinear least squares regression (Fig. 1i), enabling accurate determination of the absorbance of individual mitochondrial chromophores[30–33]. Our analysis includes a linear component with a variable slope (Fig. 1i)[34,35] to account for residual scattering and the weak absorbance by oxidized (Fe^{3+}) cytochromes, which lack spectral definition and have a lower optical density relative to the reduced hemes over this spectral range (Fig. 1e)[35]. To facilitate visualization of mitochondrial cytochromes, the linear component was subsequently subtracted from the experimental spectrum and best fit (Fig. 1j,k). Residuals, calculated as the difference between the experimental spectrum and the spectral fit, were minimal, demonstrating a good fit (Fig. 1l).

The absorbance amplitudes of hemes b_H and b_L were similar in energized mitochondria, where $\Delta\Psi_m$ is close to maximum (Fig. 1k). When $\Delta\Psi_m$ was decreased by addition of the succinate dehydrogenase (SDH) inhibitor malonate, ADP or the uncoupler BAM15, b_L became more oxidized relative to b_H, consistent with a decrease in $\Delta\Psi_m$, whereas the absolute absorbance by the *b* hemes was changed little by nigericin, which has a minor effect on $\Delta\Psi_m$ (Fig. 2a–e). Thus b_L and b_H change as anticipated in response to alterations in $\Delta\Psi_m$ in isolated mitochondria, and the derived parameter fb_L accurately reflects anticipated changes in $\Delta\Psi_m$ (Fig. 2f).

To use fb_L to quantify $\Delta\Psi_m$ in biological systems, fb_L must be calibrated against an orthogonal determination of $\Delta\Psi_m$. We measured the distribution of the lipophilic $TPMP^+$ cation across the mitochondrial inner membrane using an ion-selective electrode to precisely quantify $\Delta\Psi_m$, a long-established approach for determining $\Delta\Psi_m$ in vitro[8]. Simultaneously, we measured b_L and b_H absorbance. Mitochondria inhibited with rotenone were initially fully energized with succinate and then titrated with malonate to sequentially lower $\Delta\Psi_m$, followed by addition of the uncoupler BAM15, while fb_L and $\Delta\Psi_m$ were measured concurrently (Fig. 2g,h). To determine whether matrix pH affected the relationship between fb_L and $\Delta\Psi_m$, mitochondria respiring on succinate were treated with the ionophore nigericin, which abolishes the pH gradient, and titrated as described above (Fig. 2d,i,j). To further interrogate the relationship between fb_L and $\Delta\Psi_m$, mitochondria energized with succinate received a bolus of ADP to decrease $\Delta\Psi_m$ to a lower steady-state value, before uncoupling with BAM15 (Fig. 2k). When glutamate-malate (GM) was used as an NADH-linked electron donor, as opposed to FADH-linked succinate, $\Delta\Psi_m$ was similarly decreased with ADP (Fig. 2l). These disparate experiments enabled a calibration curve of $\Delta\Psi_m$ against fb_L to be constructed (Fig. 2m,n), showing a monotonic relationship between fb_L and $\Delta\Psi_m$ over a wide range of conditions. The sigmoidal shape of this calibration curve will make the estimation of $\Delta\Psi_m$ less certain at high and low levels where the change in fb_L is small relative to the change in $\Delta\Psi_m$. A similar relationship was observed when tetraphenylphosphonium (TPP^+) was used instead of $TPMP^+$, suggesting that either cation

https://doi.org/10.1038/s44161-025-00752-9

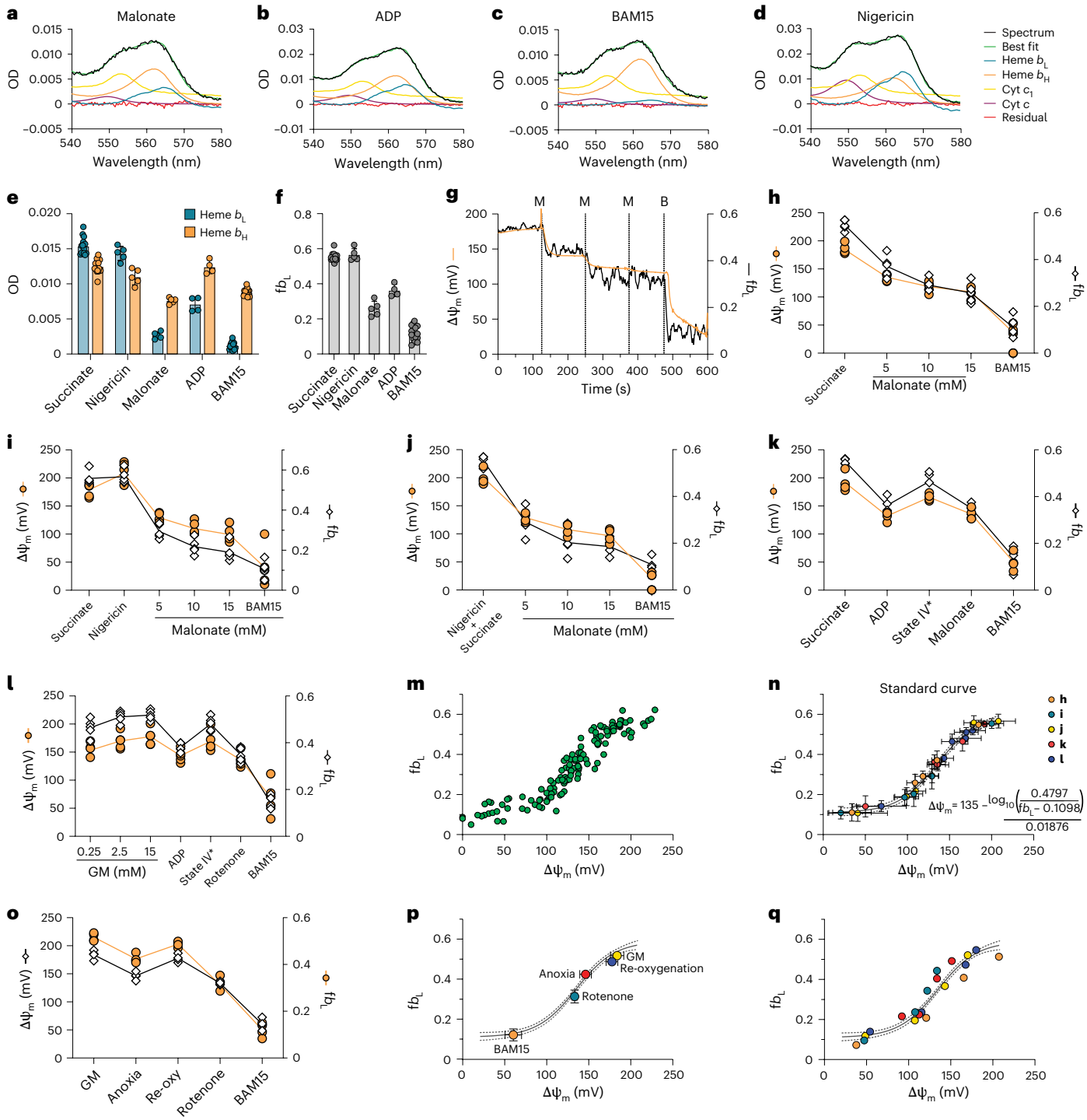

Fig. 2 | In vitro calibration of *b* heme absorbance against $\Delta\Psi_m$. **a**–**d**, Experimental absorbance spectra and best fits of mitochondria incubated with succinate/rotenone and 30 mM malonate (**a**), ADP (**b**), BAM15 (**c**) or nigericin (**d**). After spectral fitting, the linear component was subtracted from all spectra and best fits. **e**, Mitochondria were incubated with succinate/rotenone ($n = 14$) and nigericin ($n = 5$), 30 mM malonate ($n = 5$) or ADP ($n = 4$). BAM15 was added at the conclusion of all experiments ($n = 14$). Heme b_L and b_H absorbance was quantified from corresponding spectral fits. **f**, fb_L was calculated from *b* heme absorbance. **g**, Representative time course of mitochondria incubated with succinate/rotenone and titrated with malonate (M) and BAM15 (B). A rolling average of five consecutive spectra was taken before multi-wavelength nonlinear least squares regression analysis and quantification of heme b_L and b_H. $\Delta\Psi_m$, calculated from the Nernstian distribution of $TPMP^+$, and fb_L are plotted over time. **h**, fb_L and $\Delta\Psi_m$ under each condition ($n = 5$ biological replicates). **i**–**l**, Mitochondria were incubated sequentially with succinate, nigericin, malonate and BAM15 (**i**); succinate and nigericin, malonate and BAM15 (**j**); succinate, ADP, malonate and BAM15 (**k**); and GM ADP, rotenone and BAM15 (**l**). fb_L and $\Delta\Psi_m$ were determined under each condition shown. A line connects mean values. **m**, fb_L plotted as a function of $\Delta\Psi_m$ for all data points derived from **h**–**l**. **n**, Average fb_L plotted as a function of average $\Delta\Psi_m$ for all conditions shown in **h**–**l** ($n = 23$). Data were fit using nonlinear regression with a four-parameter sigmoidal model with variable slope (solid line), and 95% confidence intervals were calculated (dotted lines). **o**, Mitochondria were incubated with GM and deoxygenated by blowing N_2 over the suspension before reoxygenating 5 min later with O_2. A line connects mean values. **p**, fb_L and $\Delta\Psi_m$ were determined at each steady state shown ($n = 5$). fb_L is plotted as a function of $\Delta\Psi_m$ and superimposed onto the sigmoidal curve generated in **n**. **q**, Mouse heart mitochondria were incubated with GM followed by ADP, rotenone and BAM15, and fb_L and $\Delta\Psi_m$ were determined under each condition ($n = 5$). These data are superimposed onto the sigmoidal curve generated in **n**. Unique colors are used to represent biological replicates. All data are shown as the mean ± s.d.

can be used to monitor $\Delta\Psi_m$. To determine whether the relationship between fb_L and $\Delta\Psi_m$ is valid when the mitochondrial respiratory chain is reduced by anoxia, mitochondria incubated with GM were subjected to anoxia–reoxygenation (Fig. 2o). The unique relationship between fb_L and $\Delta\Psi_m$ was retained during anoxia (Fig. 2p) and in the presence of nigericin, which lowers the pH of the mitochondrial matrix, similar to what occurs during ischemia (Fig. 2j). Although we elected to use rabbit mitochondria, due to the amount of material required to execute these studies, we also investigated the relationship between fb_L and $\Delta\Psi_m$ in mouse heart mitochondria. We found that the calibration of fb_L to $\Delta\Psi_m$ in the mitochondria from rabbit and mouse was indistinguishable (Fig. 2q), enabling the translation of this approach to the isolated mouse heart model.

In summary, fb_L determined by optical spectroscopy is a normalized measure that responds solely to changes in $\Delta\Psi_m$ under a range of conditions, including anoxia. This development enables assessment of $\Delta\Psi_m$ in models where heme b_L and b_H absorbance can be determined, including the isolated perfused heart.

Measurement of $\Delta\Psi_m$ in the isolated heart

To determine fb_L from the reduction level of *b* hemes in the isolated mouse heart, transmural optical absorbance was measured by placing a white light-transmitting catheter inside the left ventricle (Fig. 3a). Transmitted light was collected using an integrating sphere to maximize signal by minimizing light loss due to scattering[36] (Fig. 3b). Historically, the *b* hemes have been difficult to resolve and quantify in the isolated heart due to extensive myoglobin (Mb) absorbance over the same bandwidth (Fig. 1e)[32]. To overcome this limitation, we initially used myoglobin knockout ($Mb^{-/-}$) mice, which are functionally similar to wild-type (WT) mice due to vascular compensatory mechanisms[37–40]. White light (Fig. 3c) was transmitted across the left ventricular wall, and the tissue absorbance was determined between 540 and 580 nm. Absorbance spectra (Fig. 3d) were fit with reference spectra representing reduced hemes b_H and b_L and cytochromes c_1 and *c*, along with a linear component (Fig. 3e). The residuals, calculated as the difference between experimental spectra and best fits, were minimal, indicating a good fit (Fig. 3f). To clearly visualize mitochondrial chromophores, the linear component was subtracted from the raw experimental spectrum and the best fit (Fig. 3g) after spectral fitting.

To determine whether the reduction levels of *b* hemes in the isolated heart respond as predicted to changes in $\Delta\Psi_m$, and thereby whether this approach could be used to determine $\Delta\Psi_m$, perfused hearts were challenged in series with interventions expected to alter $\Delta\Psi_m$. Hearts were perfused normally for 10 min before the sequential addition of adenosine, KCl and carbonyl cyanide-*p*-trifluoromethoxyphenylhydrazone (FCCP). Adenosine is a vasodilator and mild negative chronotrope[41] expected to suppress cardiac workload and improve oxygenation of the oxygen-limited heart, thereby increasing $\Delta\Psi_m$ (ref. 33). Cardioplegia with KCl will eliminate contractile work and is thereby also predicted to elevate $\Delta\Psi_m$, whereas uncoupling with FCCP will decrease $\Delta\Psi_m$. Tissue absorbance was measured under each condition (Fig. 3h–j), and the absorbances of hemes b_H and b_L (Fig. 3k) and cytochrome *c* (Fig. 3l) were determined from the spectral fits. The parameter fb_L was then calculated (Fig. 3m). The changes in b_H, b_L and fb_L in response to these cardioactive agents corresponded to the anticipated changes in $\Delta\Psi_m$. The calibration curve generated in isolated mitochondria (Fig. 2n) was used to calculate $\Delta\Psi_m$ from the fb_L values determined under each condition. In the isolated perfused $Mb^{-/-}$ mouse heart, $\Delta\Psi_m$ was 157 ± 14 mV ($n = 9$, mean ± s.d.) under control conditions. Adenosine decreased the heart rate from 297 ± 37 to 261 ± 46 beats per minute (bpm) and was associated with a slight increase in flow rate, whereas cardioplegia with KCl completely arrested the heart (0 ± 0 bpm; $n = 9$, mean ± s.d.). Adenosine increased fb_L to 0.59 ± 0.05 ($n = 9$, mean ± s.d.), and this was further increased following cardioplegia with KCl (0.62 ± 0.02; $n = 9$, mean ± s.d.). These values of fb_L exceeded the upper bound of the standard curve generated in isolated mitochondria, and thus, $\Delta\Psi_m$ probably exceeded 208 mV under these conditions, the highest average value of $\Delta\Psi_m$ we observed in isolated mitochondria. Uncoupling with FCCP decreased fb_L to 0.20 ± 0.04 ($n = 8$, mean ± s.d.), corresponding to a $\Delta\Psi_m$ of ~101 mV.

Cardiac $\Delta\Psi_m$ during ischemia and reperfusion

A period of ischemia substantially alters mitochondrial function and is predicted to impact $\Delta\Psi_m$. In particular, the precise kinetics and magnitude of $\Delta\Psi_m$ repolarization following prolonged exposure to ischemia are unknown. Changes in $\Delta\Psi_m$ upon reperfusion will affect the progression of tissue injury by influencing tissue energetics, ion distributions and mitochondrial ROS production. During ischemia, there is dramatic accumulation of the respiratory substrate succinate (Fig. 1b)[1,5,42]. Much of this accumulated succinate is oxidized within 1–2 min of reperfusion by the respiratory chain[42], and this has been proposed to drive the return of $\Delta\Psi_m$ to high levels shortly after reperfusion, potentially contributing to ischemia–reperfusion injury[1,5]. Our demonstration of real-time quantification of $\Delta\Psi_m$ in the isolated perfused mouse heart allows us to address this key unresolved question in ischemia–reperfusion injury[1].

To assess $\Delta\Psi_m$ changes during ischemia–reperfusion injury, $Mb^{-/-}$ mouse hearts were equilibrated under normoxic conditions and then subjected to 20 min of global ischemia, followed by 20 min of reperfusion (Fig. 4a). Tissue absorbance was recorded at 1 spectrum per second. Absorbance spectra between 540 and 580 nm were then fit with reference spectra of mitochondrial *b* hemes and cytochromes *c* and c_1, which are shown for selected time points (Extended Data Fig. 1a–d). To make continuous measurements of tissue chromophores, we took a rolling average of four absorbance spectra and then performed spectral fitting on all spectra, which enabled us to quantify b_L and b_H absorbance continuously during our ischemia–reperfusion protocol (Fig. 4b). We also measured cytochrome *c* redox state over time as an indicator of mitochondrial oxygenation status, which showed rapid cytochrome *c* reduction at the onset of ischemia followed by reoxidation immediately upon reperfusion (Fig. 4c). From continuous measurement of b_L and b_H absorbance, we determined changes in fb_L and $\Delta\Psi_m$ during ischemia–reperfusion (Fig. 4d–g).

At the onset of ischemia, $\Delta\Psi_m$ rapidly declined to a new steady-state value of 133 ± 2 mV (mean ± s.d., $n = 7$), consistent with the lack of O_2 preventing proton pumping by the respiratory chain (Fig. 4e–g). After 13 ± 2 min (mean ± s.d., $n = 7$) of ischemia, there was a further rapid decline in $\Delta\Psi_m$, which reached a minimum of 92 ± 5 mV (mean ± s.d., $n = 7$) that coincided with cardiac hypercontracture (Fig. 4e–g)[36,43]. Hypercontracture is due to the sudden sarcomere shortening that occurs when the ATP/ADP ratio falls such that dissociation of the actomyosin complex is no longer possible, causing filament contraction[43]. Upon hypercontracture after about 10 min of ischemia, we observed an apparent increase in cytochrome *c* reduction (Fig. 4c). As previously described[36], this change is consistent with an increase in the optical path length as the tissue contracts, rather than further reduction of the respiratory chain during ischemia. However, because both *b* hemes are impacted equally by changes in path length, fb_L is a normalized parameter and is unaffected by tissue geometry. We hypothesized that the presence of a relatively high $\Delta\Psi_m$ during early ischemia could be explained in part by the glycolytic supply of ATP sustaining $\Delta\Psi_m$ by reversal of the F_oF_1-ATP synthase[44–46]. Thus, inadequate production of ATP by ischemic glycolysis may explain the simultaneous occurrence of hypercontracture and the decrease in $\Delta\Psi_m$ (ref. 47). A definitive test of this hypothesis was not possible in this system due to the poor delivery of oligomycin to the mitochondria, which would have enabled inhibition of reversal of the F_oF_1-ATP synthase. Even so, depleting hearts of glycogen before the onset of ischemia led to a more rapid onset of the decline in $\Delta\Psi_m$, consistent with glycolytic ATP production sustaining $\Delta\Psi_m$ early in ischemia (Fig. 4h and Extended Data Fig. 1e).

https://doi.org/10.1038/s44161-025-00752-9

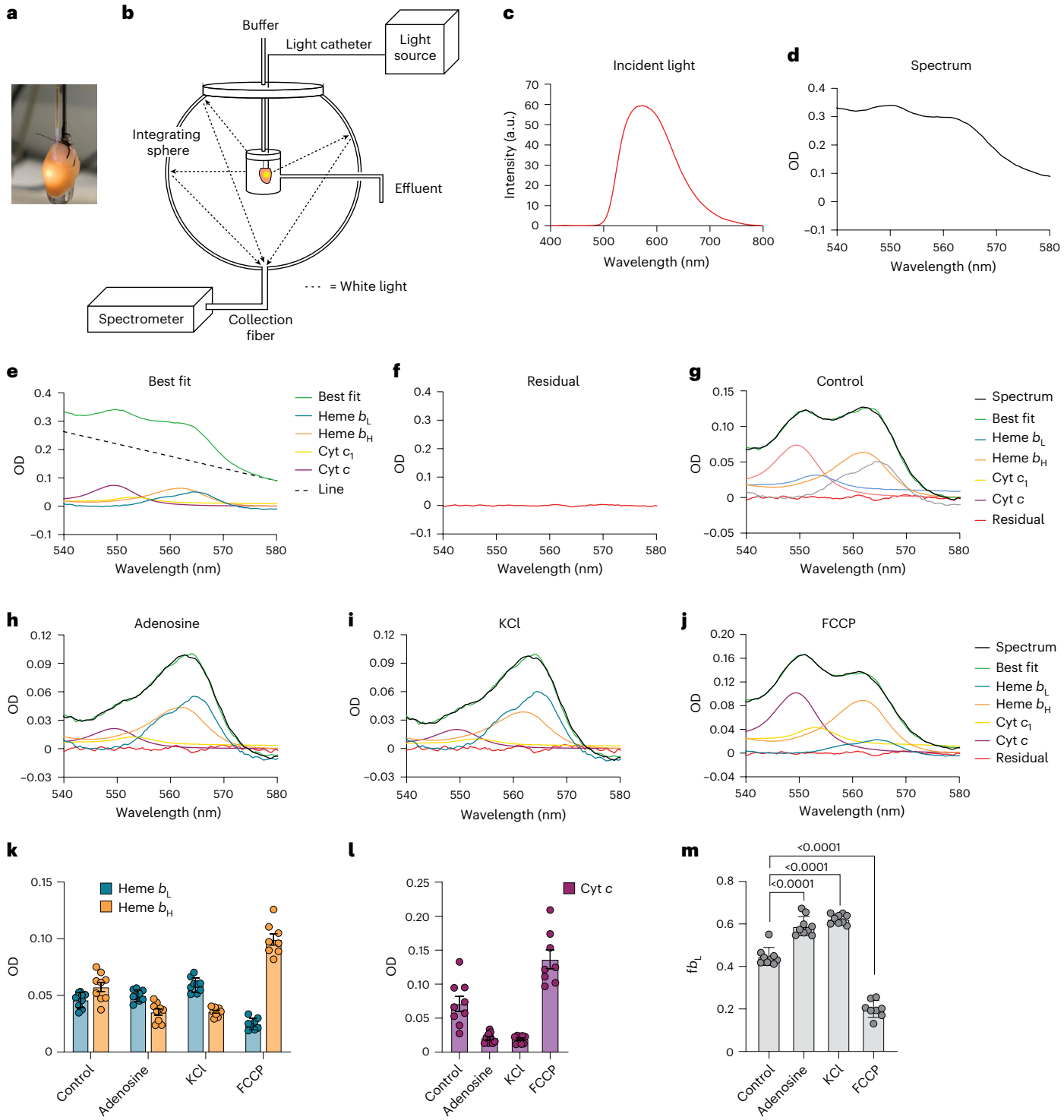

Fig. 3 | Measurement of $\Delta\Psi_m$ in the heart. a, Photograph of an isolated, perfused mouse heart with an optical light catheter (200 µm) inserted through the mitral valve and positioned in the left ventricle. **b**, Schematic of the integrating sphere system used to measure light transmittance across the left ventricular wall in real time. **c**, Incident light spectrum. **d**, The isolated perfused *Mb*$^{-/-}$ mouse heart was perfused for 20 min, and a multi-wavelength nonlinear least squares regression was performed on the experimental spectrum using reference spectra for mitochondrial hemes and cytochromes and a line. **e**, The best fit and individual chromophore contributions. **f**, The residuals of the best fit. **g**, Data in **d**–**f** with the linear component subtracted from the experimental spectrum and best fit. **h**–**j**, Isolated perfused hearts from *Mb*$^{-/-}$ mice were treated in sequence with adenosine (**h**), KCl (**i**) and FCCP (**j**) to alter $\Delta\Psi_m$. Absorbance spectra were fit by multi-wavelength nonlinear least squares regression as described above. After spectral fitting, the linear component was subtracted from all experimental spectra and best fits. **k**,**l**, Heme b_L and b_H (**k**) and cytochrome *c* (**l**) absorbances were quantified from the spectral fits ($n = 9$). **m**, fb_L was quantified from the absorbance of hemes b_L and b_H under each condition. All data are shown as the mean ± s.d. Due to one missing data point, a mixed-effects model with restricted maximum likelihood (REML) estimation was used, and fixed effects were analyzed using Dunnett's multiple comparisons test to compare treatment to control.

https://doi.org/10.1038/s44161-025-00752-9

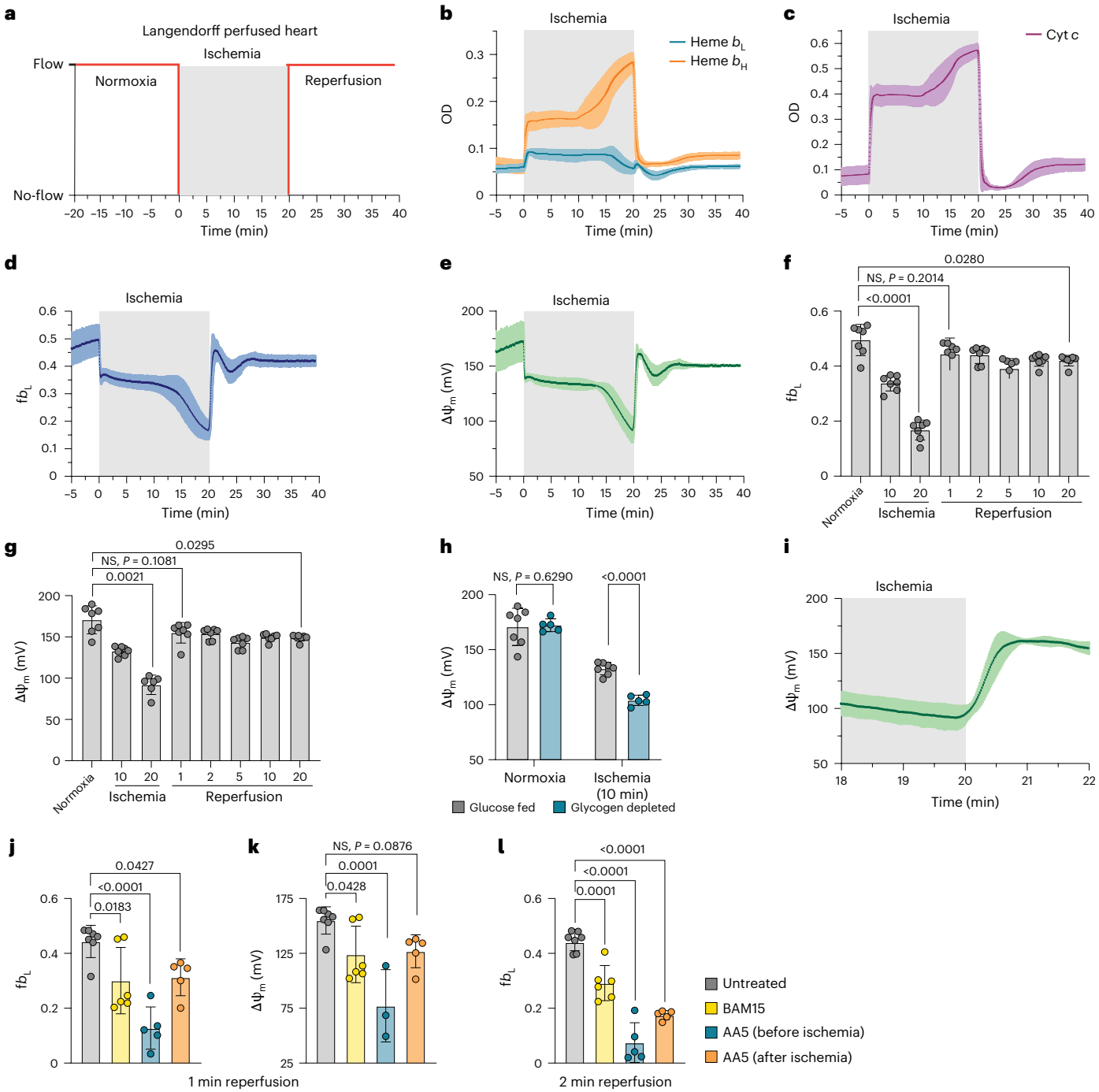

Fig. 4 | Changes in $\Delta\Psi_m$ within the heart during ischemia and reperfusion. **a**, Schematic depicting the experimental protocol for global ischemia–reperfusion in the perfused heart. **b**,**c**, Hearts from *Mb*$^{-/-}$ mice were subjected to global ischemia–reperfusion. Transmural absorbance was measured every second, and a rolling average of four consecutive spectra was taken before multi-wavelength nonlinear least squares regression analysis and quantification of hemes b_L and b_H (**b**) and cytochrome *c* (**c**) over time ($n = 7$). **d**, fb_L was quantified from the absorbances of hemes b_L and b_H, and the average fb_L was plotted over time. **e**, $\Delta\Psi_m$ was calculated from fb_L using the calibration curve generated in isolated mitochondria, and average $\Delta\Psi_m$ was plotted over time. **f**,**g**, fb_L (**f**) and $\Delta\Psi_m$ (**g**) were determined at control, 10 min or 20 min of ischemia and 1, 2, 5, 10 or 20 min of reperfusion in isolated hearts from *Mb*$^{-/-}$ mice ($n = 7$). NS, not significant. **h**, Isolated perfused *Mb*$^{-/-}$ hearts were perfused normally ($n = 7$) or with glucose-free KH buffer supplemented with sodium acetate and glucagon ($n = 5$). $\Delta\Psi_m$ was determined just before ischemia (control) or after 10 min of ischemia. **i**, Panel **e** replotted to highlight $\Delta\Psi_m$ over the first 2 min of reperfusion. **j**–**l**, Isolated hearts from *Mb*$^{-/-}$ were subjected to global ischemia–reperfusion and treated with the uncoupler BAM15 ($n = 6$) at the onset of reperfusion or the SDH inhibitor AA5 before ischemia ($n = 5$) or after ischemia ($n = 5$). fb_L (**j**) and $\Delta\Psi_m$ (**k**) were calculated after 1 min of reperfusion, and fb_L was again calculated at 2 min of reperfusion (**l**). All data are shown as the mean ± s.d. Statistical comparisons in **f**,**g**,**j**–**l** were made using one-way ANOVA with Dunnett's multiple comparisons test. Multiple unpaired two-tailed *t* tests were performed with Holm-Šídák correction for multiple comparisons to compare substrate conditions in **h**.

Upon reperfusion, cytochrome *c* was rapidly oxidized (Fig. 4c), consistent with the re-introduction of O_2 driving respiratory chain activity and leading to the reestablishment of $\Delta\Psi_m$ (Fig. 4e–g). The values of $\Delta\Psi_m$ subsequently fluctuated before stabilizing after about 10 min of reperfusion. At 20 min of reperfusion, $\Delta\Psi_m$ was significantly lower than before ischemia (Fig. 4g). These alterations in $\Delta\Psi_m$ are likely to be in response to several factors that are changing during this time, including perfusate flow, calcium redistribution, oxidative damage, initiation of cell death pathways and induction of the mitochondrial permeability transition pore (MPTP), which will be explored in the future. Focusing on reperfusion, we observed rapid repolarization over the first 60 s of reperfusion (Fig. 4i), with $\Delta\Psi_m$ reaching the same value as that at normoxia, before ischemia (Fig. 4g). This initial repolarization was blocked by the uncoupler BAM15 (Fig. 4j–l and Extended Data Fig. 1f), consistent with proton pumping by the respiratory chain driving repolarization. To further interrogate the contribution of succinate-driven respiratory chain proton pumping to the reestablishment of $\Delta\Psi_m$, we pretreated the hearts with the irreversible SDH inhibitor atpenin A5 (AA5), which prevented $\Delta\Psi_m$ hyperpolarization (Fig. 4j–l and Extended Data Fig. 1g). The addition of AA5 upon reperfusion also dampened repolarization, although this effect was smaller (Fig. 4j–l and Extended Data Fig. 1h). As SDH is a component of the citric acid cycle (TCA), the effect of AA5 may not be limited to succinate oxidation. Despite the variability observed in $\Delta\Psi_m$ at 1 min of reperfusion following the addition of either BAM15 or AA5 after ischemia, we observed a progressive decline in $\Delta\Psi_m$ between 1 min and 2 min of reperfusion (Fig. 4l) consistent with slow and variable uptake and subsequent target engagement of these hydrophobic compounds[48] relative to the fast rates of repolarization (Fig. 4i).

Having confirmed the feasibility of this approach in *Mb*$^{-/-}$ mouse hearts, isolated hearts from WT mice were subjected to global ischemia–reperfusion. Hearts from WT mice had, as expected, greater absorbance than those from *Mb*$^{-/-}$ mice due to Mb (Fig. 5a). Experimental spectra from WT hearts (Fig. 5b–d and Extended Data Fig. 2a–d) were deconvolved using reference spectra for oxygenated (MbO) and deoxygenated (MbD) Mb in conjunction with the mitochondrial cytochrome reference spectra used previously for the *Mb*$^{-/-}$ hearts. In the case of the WT mouse heart, absorbance of b_L and b_H and cytochrome *c*, as well as MbO and MbD, was quantified from the spectral fits (Fig. 5e–g), and fb_L was determined at selected time points (Fig. 5h), rather than continuously due to the low signal-to-noise ratio observed in the WT heart. fb_L followed a similar profile during ischemia and reperfusion as in hearts from knockout mice (Fig. 5h), and indeed, $\Delta\Psi_m$ values for WT and *Mb*$^{-/-}$ hearts were the same under these conditions (Fig. 5i).

The above data were collected in WT hearts perfused with Krebs–Henseleit (KH) buffer containing glucose only. To evaluate the influence of substrate availability on the trends observed, we repeated these experiments in hearts perfused with glucose, lactate, pyruvate and butyrate and obtained similar results (Fig. 5j,k). Thus, we were able to quantify and characterize $\Delta\Psi_m$ during ischemia and reperfusion in the isolated perfused heart. Together, these data show that maximal $\Delta\Psi_m$ is rapidly reestablished upon reperfusion due to the restoration of respiration from carbon substrates in the presence of O_2.

Metabolic changes during ischemia and reperfusion

We next investigated whether the energetic and metabolic status of the mitochondria during ischemia–reperfusion is consistent with oxidation of the succinate accumulated during ischemia by SDH upon reperfusion. The rapid hyperpolarization of $\Delta\Psi_m$ upon reperfusion (Fig. 4i) and its prevention by the SDH inhibitor AA5 (Fig. 4k) are consistent with rapid oxidation of the accumulated succinate. However, it is also important to consider mitochondrial redox status, oxygen tension and respiratory activity. Therefore, we further interrogated how these other factors changed upon reperfusion of the ischemic heart. We found that cytochrome *c* was oxidized within 60 s of reperfusion (Figs. 4c and 5f). In the WT heart, Mb was reoxygenated within 60 s of reperfusion (Fig. 5g). Together, these findings are consistent with the rapid reoxygenation of the heart tissue and reestablishment of respiration, enabling proton pumping and the regeneration of $\Delta\Psi_m$. These data also confirm that mitochondrial oxygen tension is sufficient for both respiration and the production of ROS early after reperfusion. Assessing the levels of succinate in the isolated perfused *Mb*$^{-/-}$ and WT hearts during ischemia–reperfusion showed the expected accumulation of succinate during ischemia[5,49], followed by its rapid return to pre-ischemic levels within 2 min of reperfusion (Fig. 6a). The rapid removal of succinate observed is consistent with its oxidation by SDH upon reperfusion, as well as some release from cardiomyocytes via the monocarboxylate transporter 1 (refs. 50–52). We assessed the redox state of the CoQ pool by measuring its percentage reduction by liquid chromatography followed by tandem mass spectrometry (LC–MS/MS)[53], which showed that the CoQ pool became highly reduced during ischemia and was then oxidized back to normoxic levels within 1 min of reperfusion (Fig. 6b). Over the next 4 min, the CoQ pool became more oxidized than the control before becoming gradually more reduced over the subsequent 15 min (Fig. 6b). This observed change in redox poise of the CoQ pool upon reperfusion is consistent with its oxidation by complex III to facilitate proton pumping at complexes III and IV to support the reestablishment of $\Delta\Psi_m$. Additionally, some $CoQH_2$ may be oxidized by acting as a chain-breaking antioxidant to limit lipid peroxidation within the mitochondrial inner membrane[54].

Combining these measures of mitochondrial function showed that they correlated over the crucial first minutes of reperfusion (Fig. 6c,d). Several important points emerged from these temporal comparisons. Respiration, and thus proton pumping by the respiratory chain, switched on within seconds as O_2 was reintroduced into the ischemic heart, as indicated by the changes to cytochrome *c* and Mb absorbance. This activation of respiration correlated with the rapid increase in $\Delta\Psi_m$ and with depletion of the accumulated succinate. The succinate oxidation was able to sustain a partially reduced CoQ pool over the first minutes of reperfusion. These findings confirm that $\Delta\Psi_m$ repolarization occurs at the onset of reperfusion supported by succinate oxidation, consistent with a central contribution of a large $\Delta\Psi_m$ to the initiation of ischemia–reperfusion injury.

Discussion

The maintenance of $\Delta\Psi_m$ is critical to mitochondrial function and cell integrity. Until now, it has not been possible to quantify $\Delta\Psi_m$ in real time in the intact heart. Here, we exploited the biophysical properties of the *b* hemes of the cytochrome bc_1 complex, which enabled us to relate the optical absorbance of hemes b_L and b_H to $\Delta\Psi_m$. From the absorbance of *b* hemes, we generated a normalized parameter fb_L that was stable over a range of conditions and could be calibrated against $\Delta\Psi_m$. Using this procedure, we were able to quantify $\Delta\Psi_m$ in real time within the intact heart to investigate normal cardiac physiology and also to assess the impact of cardiac ischemia–reperfusion on $\Delta\Psi_m$. This approach overcomes the many limitations associated with the use of exogenous probes, dyes and tracers because the *b* hemes are stably expressed and localized within the mitochondrial inner membrane. Additionally, electron exchange between the *b* hemes, and thus alterations in optical absorbance, occurs on the order of microseconds[55], which enables close to real-time quantification of $\Delta\Psi_m$. Many other in vitro or ex vivo models can be adapted to use this approach to assess how $\Delta\Psi_m$ contributes to cardiac physiology and pathology.

Combining all measurements from WT and *Mb*$^{-/-}$ hearts, $\Delta\Psi_m$ was 166 ± 18 mV (n = 25, mean ± s.d.) in the nonworking, saline-perfused mouse heart under control conditions. How do these measures in the intact perfused heart relate to the mitochondrial Δp in the heart in vivo? The low workload and somewhat restricted oxygen delivery of the saline-perfused mouse heart make it challenging to extrapolate these measurements to the in vivo working heart. Even so, after vasodilation

https://doi.org/10.1038/s44161-025-00752-9

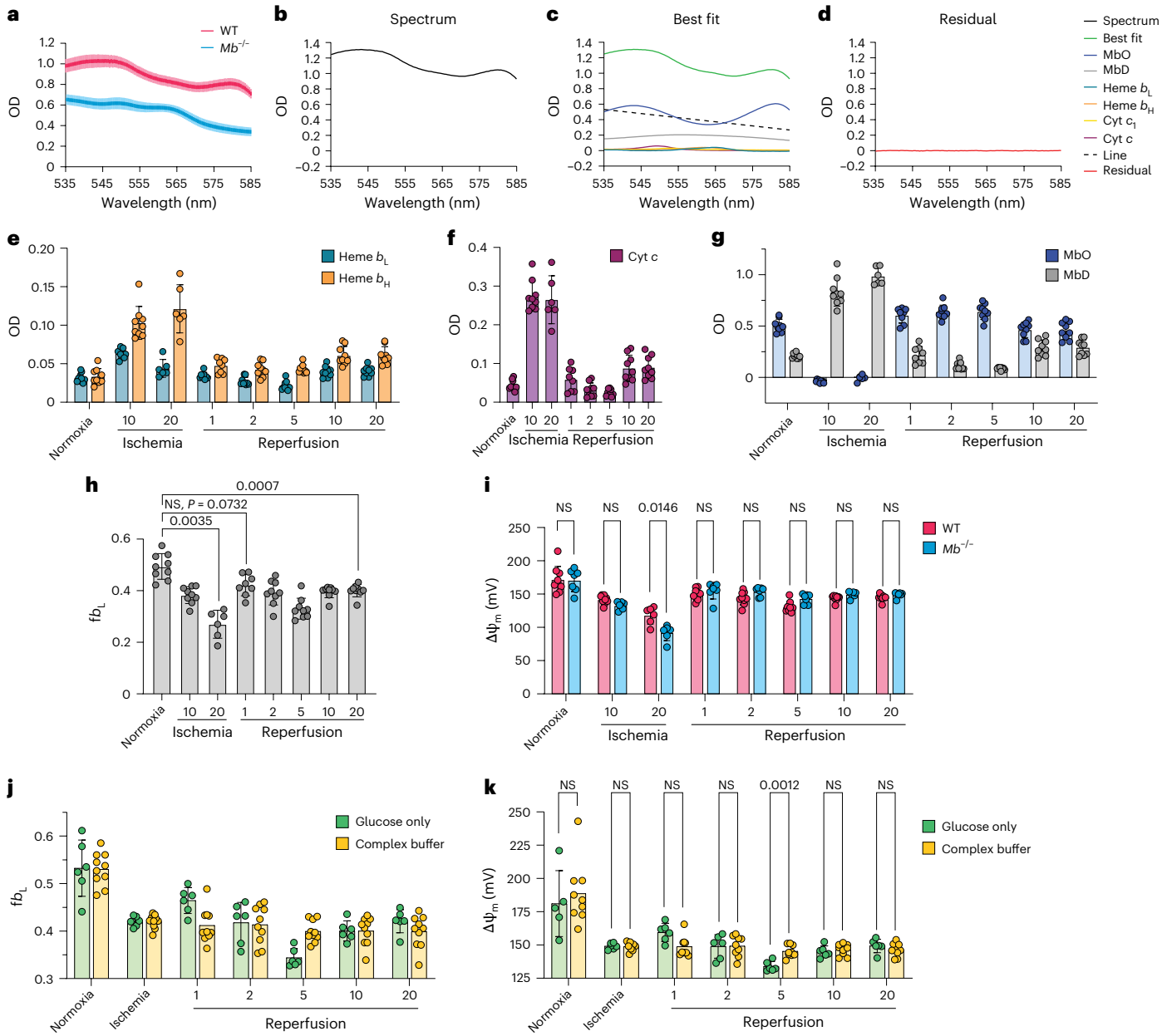

Fig. 5 | Changes in $\Delta\Psi_m$ within the WT heart during ischemia and reperfusion. Isolated perfused C57BL/6N mouse hearts were subjected to global ischemia–reperfusion ($n = 9$). **a**, Average transmural absorbance of isolated perfused hearts from WT or $Mb^{-/-}$ mice under control conditions ($n = 3$ each). **b**, Transmural absorbance was determined under normoxic conditions, and a multi-wavelength nonlinear least squares regression was performed using reference spectra for hemes b_L and b_H and cytochromes c_1 and c, as well as MbO and MbD, and a line. **c**, The best fit and individual chromophore contributions. **d**, The residual of the best fit. **e**–**g**, The absorbances of hemes b_L and b_H (**e**), cytochrome c (**f**) and MbO and MbD (**g**) were quantified from the spectral fits at selected time points. Four data points from three biological replicates were excluded due to low spectral signal-to-noise ratio. **h**, fb_L was calculated as previously described. **i**, Comparison of $\Delta\Psi_m$ at selected time points in isolated hearts from WT ($n = 9$) or $Mb^{-/-}$ ($n = 7$) mice subjected to global ischemia–reperfusion. **j**,**k**, Isolated hearts from WT mice were perfused with KH buffer containing glucose only ($n = 6$) or glucose, lactate, pyruvate and butyrate (complex buffer) ($n = 10$) and subjected to global ischemia–reperfusion. Multi-wavelength nonlinear least squares regression was performed on the experimental spectra collected at selected time points, and fb_L (**j**) and $\Delta\Psi_m$ (**k**) were calculated as previously described. Due to missing data points, a mixed-effects model with REML estimation was used in **h**, and fixed effects were analyzed using Dunnett's multiple comparisons test to compare selected time points to control. Multiple unpaired two-tailed t tests with a Holm-Šídák correction were used to compare genotypes in **i** and substrate conditions in **k**. All data are shown as the mean ± s.d.

with adenosine, $\Delta\Psi_m$ surpassed ~200–210 mV, which may better reflect the in vivo condition where oxygen delivery is optimal, as evidenced by nearly complete Mb saturation[56,57]. Cardioplegia after vasodilation slightly enhanced fb_L, suggesting that this condition approaches the maximal value of $\Delta\Psi_m$ attainable. These maximum values of $\Delta\Psi_m$ are higher than those usually reported for isolated mitochondria. This may be due in part to the fact that the retrogradely perfused heart is only doing rate work with no load, so the metabolic rate is more than tenfold lower than that with the maximum possible workload[58]. Thus, the unloaded heart that we interrogate here is much closer to state 4 than state 3. It is also important to note that preparations of isolated mitochondria are typically 0.8- to 1-µm spheres that arise from the shearing and resealing of the mitochondria present in tissues, which in the heart are primarily long, thin structures many micrometers in length[59]. It may be that the inner membranes of isolated mitochondria are thus more susceptible to proton leak than those of undisturbed

https://doi.org/10.1038/s44161-025-00752-9

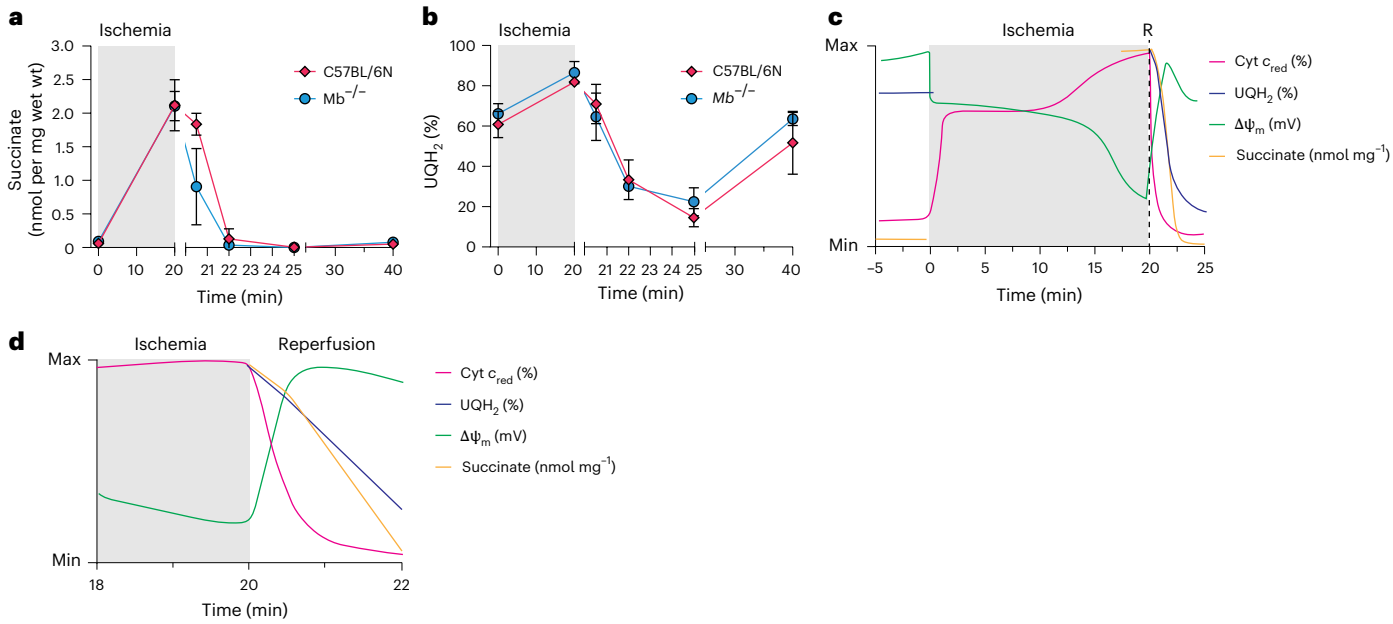

Fig. 6 | Metabolic changes during ischemia and reperfusion. Isolated perfused C57BL/6N or *Mb*$^{-/-}$ mouse hearts ($n = 6$) were subjected to global ischemia–reperfusion. Whole hearts were rapidly frozen at control, after 20 min of ischemia or the indicated times after reperfusion. **a**, Succinate was extracted from frozen tissue samples and measured by LC–MS/MS against a [$^{13}C_4$]succinate internal standard. **b**, $CoQH_2$ and CoQ were extracted from frozen tissue, and the percent reduction was determined by LC–MS/MS by determining the proportion of $CoQH_2$ relative to total CoQ and $CoQH_2$. **c**, Succinate and $CoQH_2$ data from **a** and **b** were fit to interpolated curves and are plotted over time along with cytochrome *c* absorbance (Fig. 4c) and $\Delta\Psi_m$ (Fig. 4i). **d**, Curves in **c** replotted to highlight reperfusion. The *y* axes of **c** and **d** represent the range of values observed in the heart in this study. Data presented in **a** and **b** are the mean ± s.d.

mitochondria in intact tissue, possibly resulting in a more polarized maximum membrane potential in the perfused heart.

To determine Δp ($\Delta\Psi_m - 61.5\,\Delta pH$), the magnitude of ΔpH ($pH_{cytosol} - pH_{matrix}$) must be known; however, its value in the intact heart remains unclear. ΔpH amplitudes of −0.4 (ref. 60) and of −0.2 (ref. 61) have been reported in isolated mouse cardiomyocytes. These estimations suggest that ΔpH contributes 12–28 mV to the Δp; however, further work is required to experimentally determine ΔpH values in the intact heart. Allowing for this gap in our knowledge, the in vitro ΔpH values give an estimate for Δp of 178–194 mV in the isolated perfused heart. A similar extrapolation, with related caveats, suggests maximal values of Δp of ~212–228 mV in the in vivo working heart.

The ability to measure $\Delta\Psi_m$ in real time enabled us to assess how this parameter changes in a mouse heart model of global ischemia–reperfusion. Our analysis indicated that upon reperfusion of the ischemic heart, $\Delta\Psi_m$ was reestablished to normoxic levels within 1 min, suggesting that the capacity to synthesize ATP by oxidative phosphorylation is rapidly restored. The reestablishment of $\Delta\Psi_m$ correlated with the oxidation of the succinate accumulated during ischemia and maintenance of a partially reduced CoQ pool. These data are consistent with a model of ischemia–reperfusion injury in which mitochondrial superoxide production occurs at complex I by reverse electron transport (RET) at the onset of reperfusion[1,5], initiating the oxidative damage that in turn leads to induction of the MPTP, cell death and the release of damage-associated molecular patterns (DAMPs) that activate the innate immune response. However, the timing and ordering of ROS production and induction of the MPTP are currently unresolved[14,15,17,50]. Future work will address this by assessment of $\Delta\Psi_m$ over the several minutes of reperfusion along with parallel measurement of ROS production, mitochondrial Ca^{2+}, pH and induction of the MPTP.

There are a number of considerations that potentially constrain the implications of this study that will be addressed in future work. Our approach assumes that the relationship between fb_L and $\Delta\Psi_m$ is similar in vitro and in vivo and that the quantification of $\Delta\Psi_m$ based on $TPMP^+$ or TPP^+ distribution is accurate. The optical approach using measurement of b_L and b_H provides a global measurement of the average $\Delta\Psi_m$ in the mitochondria within the light paths interrogated, much like global ^{31}P or ^{13}C nuclear magnetic resonance studies. Therefore, this approach does not provide information about heterogeneous cellular responses to ischemia–reperfusion injury, which likely dictate individual cell fate; instead, these measurements reflect the average of all cardiomyocytes assessed. It should also be noted that the estimates of $\Delta\Psi_m$ reported herein were obtained using a nonworking isolated heart model, which does not reflect the in vivo workload. Furthermore, accurate determination of the contribution of ΔpH to the value of Δp is required. To do this will require the extension of real-time optical techniques to assess the pH of the cytosol and mitochondrial matrix under steady-state conditions and particularly during ischemia and reperfusion when the pH changes rapidly.

In summary, we have developed a method to quantify $\Delta\Psi_m$ in real time within the intact, perfused mouse heart. We used this approach to determine the value of $\Delta\Psi_m$ within the heart under normoxic conditions and then assessed the rate of reenergization of the mitochondria upon reperfusion, providing new insights into the contribution of the mitochondria to ischemia–reperfusion injury. This approach opens the way to assessing many other aspects of how the mitochondria contribute to cardiac pathophysiology.

Methods

Ethical approval

All animal protocols were approved by the Animal Care and Use Committee at the National Heart, Lung and Blood Institute, National Institutes of Health, Bethesda, USA, and were performed in accordance with the guidelines described in the Animal Welfare Act.

Animal experiments

Male New Zealand white rabbits (Charles River) were singly housed with ad libitum access to food and water. Female and male mice were housed separately with ad libitum access to food and water. C57BL/6N mice (Taconic) were acclimatized for at least 7 days before experimentation.

Mouse models

Mb$^{-/-}$ mice were provided by C. Noguchi (National Institute of Diabetes and Digestive and Kidney Diseases)[40].

Isolation of mitochondria from rabbit heart

Male New Zealand white rabbits (6–12 months) received an intramuscular injection of ketamine (100 mg ml^{-1}) and acepromazine (10 mg ml^{-1}) followed by a mixture of medical air and O_2 containing 3% isoflurane via inhalation. After confirming anesthesia by toe pinch, 1,500 units of USP-grade heparin was administered intravenously. Rabbits were killed by intravenous bolus of KCl (6 mEq), and the heart was rapidly excised and flushed with modified KH buffer containing (in mM) 137 NaCl, 10 HEPES, 5.4 KCl, 1.8 $CaCl_2$, 0.5 $MgCl_2$, 0.5 Na_2HPO_4, 10 glucose and 1 lactate (pH 7.4) and 1,000 units of USP-grade heparin. The mitochondrial isolation preparation procedure previously reported for dog and pig heart[58] was modified as follows. The heart was dissected of atria, fat and connective tissue, and the remaining tissue was diluted to 20% (w/v) in cold isolation buffer containing (in mM) 10 HEPES, 5 K_2HPO_4, 1 EDTA, 1 EGTA and 280 sucrose (pH 7.1). The tissue was minced and diluted to 70 ml before mechanical homogenization (Virtis) on ice for 20 s at 40% power. Suspensions were digested with trypsin (0.5 mg per g tissue) for 15 min at 4 °C, and digestion was stopped with trypsin inhibitor (2.6 mg per g tissue) and 100 mg BSA. The suspension was centrifuged at 600*g* for 10 min at 4 °C, and the supernatant was collected. The pellet was resuspended with isolation buffer and homogenized using two passes of a 1-mm-clearance Dounce followed by five passes of a 0.2-mm-clearance Dounce. The homogenate was centrifuged at 600*g* for 10 min at 4 °C, and the supernatant was combined with the first isolate. The pellet was resuspended and pelleted at 600*g* twice more, collecting the supernatant each time. The pooled supernatant was centrifuged at 8,000*g* for 10 min at 4 °C, and the mitochondrial pellet was resuspended in isolation buffer and pelleted again at 8,000*g* for 10 min. The pellet was resuspended in Fiskum buffer containing (in mM) 125 KCl, 20 HEPES, 15 NaCl, 5 $MgCl_2$, 5 K_2HPO_4, 1 EGTA and 1 EDTA, pH 7.1, and centrifuged once more at 8,000*g* for 10 min at 4 °C. This pellet was resuspended in Fiskum buffer and purified by Percoll gradient. The layer containing intact mitochondria was resuspended in Fiskum buffer and centrifuged at 13,000*g* for 10 min at 4 °C. The pellet was resuspended and centrifuged at 10,000*g* for 10 min at 4 °C. The final pellet was resuspended in 1 ml Fiskum buffer.

The fully reduced cytochrome $a + a_3$ content was quantified assuming an extinction coefficient of 12 mM^{-1}cm^{-1} for the reduced minus oxidized cytochrome $a + a_3$ at 605 nm[62]. A 25-µl aliquot of mitochondria was added to 1 ml of 2% Triton X-100 buffer. An oxidized spectrograph was collected, and then 10 mM sodium dithionite was added followed by collection of a reduced spectrograph; the difference at 605 nm was determined, and the concentration of cytochrome oxidase was quantified. The average cytochrome $a + a_3$ content in these preparations was 43.7 ± 1.5 nmol ml^{-1}. Protein concentration was determined by Bradford assay (1856209, Thermo) using an albumin standard (23209, Thermo). The average protein concentration in these preparations was 23.9 ± 0.9 mg ml^{-1}.

Isolation of mitochondria from mouse heart

Mitochondria from eight C57BL/6N mouse hearts were isolated by mechanical homogenization and trypsin digestion and separated by differential centrifugation as previously described[63] in isolation buffer containing (in mM) 225 mannitol, 75 sucrose, 5 MOPS, 0.5 EGTA and 2 taurine (pH 7.25). Cytochrome oxidase content was quantified as described above. Mitochondria (5–7 nmol cytochrome $a + a_3$) were suspended in 5 ml Fiskum buffer containing (in mM) 125 KCl, 20 HEPES, 15 NaCl, 5 $MgCl_2$, 5 K_2HPO_4, 1 EDTA, 0.6 EGTA and 0.25 $CaCl_2$. Mitochondria were incubated sequentially with 5 mM GM, 0.5 mM ADP, 5 µM rotenone and 2 µM BAM15, and at least 50 samples were averaged for optical or TPMP$^+$ uptake measurements.

Mitochondrial absorption spectroscopy

A custom-made cylindrical glass chamber (15 mm in diameter × 50 mm in height) (Chemglass) was mounted to a scaffold attached to the lid of an integrating sphere (RTC-060-SF, LabSphere). A magnetic stirrer (SCS 1.11, Starna Spinette) was secured to the bottom of the scaffold, and the isolated mitochondrial suspensions were gently stirred. Light was supplied by a tungsten bromide light source and directed at the suspension at a 90° angle (LLC-10A, Lambda Scientific) via an optical fiber (FT1000UMT, Thor Labs). Transmitted light was focused to the bottom of the integrating sphere by three uniquely positioned baffles. Transmitted light was collected using an optical fiber (FT1000UMT, Thor Labs) connected to a cooled, rapid-scanning spectrometer (QEPro, Ocean Optics). The intensity of the light source without mitochondria present (I_0) and the dark current of the spectrometer were collected at the start of each day. Transmitted light was recorded at 1,044 points between 348 and 745 nm at one sample per second using a custom LabVIEW-based program[32].

Isolation of cytochrome bc_1 complex

Isolated rabbit heart mitochondria were diluted to 10 nmol cytochrome $a + a_3$ per ml in isolation buffer containing 50 mM Tris and 1 mM $MgSO_4$, adjusted to pH 8.45, at 4 °C. While mixing gently on ice, 10% (w/v) *n*-dodecyl β-D-maltoside (DDM) was added to 1% (w/v). The suspension was centrifuged at 40,000*g* for 40 min at 4 °C. The supernatant was transferred to a 2.5 × 20 cm glass column (Bio-Rad) containing DEAE Sepharose Fast Flow anion exchange resin (GE Healthcare) washed and equilibrated with isolation buffer C containing 0.02% (w/v) DDM. The column was eluted twice with ~4 ml isolation buffer C containing 0.02% (w/v) DDM before mitochondrial complexes were eluted by applying a linear NaCl gradient between 0 and 400 mM. The reddish-brown fractions eluted between 290 mM and 400 mM NaCl containing cytochrome bc_1 were concentrated using an Amicon Ultra-15 centrifugal filter (Millipore) with a 10-kDa membrane cutoff and then diluted with 50% (v/v) glycerol and 0.1% lauryl maltoside.

Collection of heme and cytochrome reference spectra

Reference spectra for hemes b_L and b_H and cytochromes c_1 and *c* were collected in the integrating sphere. Purified cytochrome *c* (equine heart; C2506, Sigma-Aldrich) (1.5 nmol ml^{-1}) was added to 5 ml Fiskum buffer, and the absolute absorbance spectrum of reduced cytochrome *c* was recorded after the addition of 5 mM sodium ascorbate.

To determine the absorbance spectrum of cytochrome c_1, isolated complex III (7.1 nmol cytochrome *b* ml^{-1}) was added to 5 ml Fiskum buffer. After recording the fully oxidized spectrum, 10 mM sodium ascorbate was added, and the absolute reduced cytochrome c_1 reference was estimated by subtracting 66% of the oxidized absorbance to remove the spectral contributions from oxidized b_H and b_L. The same sample was then titrated with 50 µl sodium dithionite (10% (w/v) in dH_2O) to selectively reduce heme b_H, as confirmed by the absence of both the peak at 566 nm and a shoulder at 558 nm that correspond to the b_L heme[34,35]. The b_H absolute reduced reference was obtained by subtracting the absolute cytochrome c_1 reduced reference. This reference was determined to be accurate based on the negligible cytochrome c_1 contribution in the Soret spectral region at 410 nm.

To collect the reference spectrum for heme b_L, isolated mitochondria (2 nmol ml^{-1}cytochrome $a + a_3$) were added to 5 ml Fiskum buffer and made anoxic by incubating with 20 mM GM and 5 mM ADP while N_2 was blown over the suspension. FCCP (0.5 µM) was then added to the suspension. The heme b_L reference was determined by taking the difference in absorbance between anoxia and after FCCP. The reference for heme b_L represents the difference between the reduced and oxidized species but is predicted to closely represent the shape of the absolute reduced absorbance spectrum, considering that the absorbance of oxidized heme b_L is nearly constant over this spectral bandwidth.

Collection of myoglobin reference spectra

One C57BL/6N mouse heart was flushed with KH buffer containing 1,000 units USP-grade heparin and transferred into 50 mM HEPES on ice once fat, atria and connective tissue were dissected away. The heart was diluted to 20% (w/v), minced with scissors and then centrifuged at 10,000*g* for 10 min at 4 °C. The supernatant containing Mb was transferred to a 2-ml Eppendorf tube on ice. The absorbance of the oxygenated sample was measured between 400 and 750 nm (UV-2700, Shimadzu) before treatment with 10 mM sodium dithionite (10% (w/v) in dH_2O) to deoxygenate.

Spectral analyses

Spectra collected using a custom LabView-based program were converted to.csv files containing all wavelengths, I_0, dark current and all transmission spectra. Optical data were analyzed using custom R scripts. Absorbance was calculated as the $\log_{10}$-transformed ratio of the incident to transmitted light. Absorbance data collected from isolated mitochondria or $Mb^{-/-}$ mice were fit between 540 and 580 nm with reference spectra for hemes b_L and b_H and cytochromes c_1 and c, together with a line, using a nonlinear least squares regression fitting routine. The model is described by equation (1) where a–f represent unique fitting coefficients. The fitted model describes the experimental absorbance spectrum as a combination of linear contributions from different spectral components and a linear component with variable slope and intercept.

$$\begin{aligned}\text{Absorbance} = (\text{heme}b_H \times a) + (\text{heme}b_L \times b) + (\text{cyt}c_1 \times c) \\ +(\text{cyt}c \times d) + (\text{wavelength} \times e + f)\end{aligned} \quad (1)$$

Nonlinear least squares regression was conducted using routines for nonlinear least squares optimization in the minpack.lm package (https://www.rdocumentation.org/packages/minpack.lm/versions/1.2-4). Least squares analysis of the bc_1 complex was previously shown to be superior to absorbance peak analysis[64], including in the perfused heart[32,65]. To calculate the absorbance of individual hemes and cytochromes, the fit coefficient generated by the nonlinear least squares regression was multiplied by the optical density of the original reference spectrum at every wavelength.

Determination of $\Delta\Psi_m$ in isolated mitochondria

A TPP^+-selective electrode (World Precision Instruments) filled with 10 mM $TPMP^+$ and a reference electrode (MI-402, Microelectrodes) filled with 3 M KCl were conditioned in 100 mM NaCl. The $TPMP^+$-selective and reference electrodes were placed into the mitochondrial suspension, and electrode voltages were measured with a pH millivolt meter (PH-1, Microelectrodes). Isolated mitochondria were incubated with 5 µM rotenone or without substrate for 15 min to de-energize mitochondria. The electrode was then calibrated in the presence of mitochondria by making six $TPMP^+$ additions up to 2.17 µM. Electrode voltage was recorded at one sample per second. The changes in external $TPMP^+$ were assessed and used to calculate the amount of $TPMP^+$ sequestered by mitochondria, assuming a starting concentration of 2.17 µM and bath volume of 5.5 ml. The free concentration of $TPMP^+$ was calculated by dividing the amount of $TPMP^+$ taken up by mitochondria by the amount of mitochondrial protein added and then multiplied by the binding correction of 0.17 mg protein μl^{-1}(ref. 8). $\Delta\Psi_m$ was calculated by the Nernst equation: $61.5 \log_{10} [TPMP^+]_{in}/[TPMP^+]_{out}$ (mV).

Studies of mitochondria isolated from rabbit heart

Mitochondria (2 nmol ml^{-1}cytochrome $a + a_3$) were added to Fiskum buffer supplemented with 0.6 mM $CaCl_2$. O_2 was gently blown over the surface unless otherwise noted. Mitochondria were incubated with 5 µM rotenone or starved before $TPMP^+$ calibration as described above. Mitochondria incubated with 5 mM succinate (pH 7.0) were titrated with malonate up to 30 mM (pH 7.0) or 2 mM ADP (pH 7.0). To study the effect of pH, 1 µM nigericin was added to mitochondria incubated with 5 µM rotenone before $TPMP^+$ calibration, or after the addition of succinate, and then titrated with malonate as described above. Mitochondria incubated with GM (pH 7.0) were similarly incubated with ADP until all ADP was converted into ATP (annotated state IV*). In succinate-fed mitochondria incubated with ADP, 10 mM malonate was added after state IV* to inhibit respiration. In GM-fed mitochondria, 5 µM rotenone was added instead. Mitochondria were uncoupled with 2 µM BAM15. To study anoxia–reoxygenation, mitochondria were incubated with 10 mM GM for 5 min before O_2 was removed by gently blowing N_2 over the surface of the suspension. Mitochondria were incubated under anoxic conditions for 5 min before O_2 was reintroduced followed by 5 µM rotenone and 2 µM BAM15.

Langendorff perfusion

Male or female C57BL/6N or $Mb^{-/-}$ mice between 9 and 16 weeks of age were anesthetized (50 mg sodium pentobarbital) and administered 100 units of USP-grade heparin by intraperitoneal injection. After determining the depth of anesthesia, the heart was excised and submerged in ice-cold KH buffer with (in mM) 120 NaCl, 25 $NaHCO_3$, 4.7 KCl, 1.75 $CaCl_2$, 1.2 $MgSO_4$, 1.2 KH_2PO_4 and 10 D-glucose that had been filtered (0.22 µm) before use. After excision, the heart was cannulated and retrogradely perfused at constant pressure (90 mm Hg) with KH buffer maintained at 37 °C and bubbled with 95% O_2/5% CO_2 (pH 7.4). The coronary sinus was not cannulated. For optical studies, the left atrium was removed, and a light catheter (FIP200220240, Molex) was positioned inside the left ventricular cavity. The heart was then secured in a water-jacketed glass chamber maintained at 37 °C. For tissue collection, the heart was submerged in a glass reservoir filled with KH buffer maintained at 37 °C. In all studies, the effluent flow rate was measured continuously using a flow-through sensor (1PXN, Transonic) placed before the heart, coupled to a Tubing Flow Module (TS410, Transonic). Temperature was measured using a flexible temperature microprobe (IT-18, AD Instruments). Flow and temperature signals were digitized via a PowerLab interface (AD Instruments). Flow was recorded at 1,000 samples per second, and heart rate was calculated based on the sinusoidal flow rate with the peak of each wave taken to be one beat and the number of peaks calculated over time.

Myocardial optical absorption spectroscopy and analysis

The water-jacketed glass chamber harboring the isolated heart was positioned inside an integrating sphere, using a 6-inch-diameter integrating sphere (RTC-060-SF, LabSphere). Light was supplied by a 560-nm broadband white light source (LCS 0560-68-22, Mightex) powered by a BioLED Light Source Control Module (BLS-Series, Mightex). Transmitted light was collected using a multimode optical fiber (FT1000UMT, Thor Labs) fitted to the bottom port of the LabSphere and measured by a cooled, rapid-scanning spectrometer (VIS-A-S-100, Wasatch Photonics). The light intensity without tissue and dark current of the spectrometer were collected at the start of each day. Light intensity was recorded at 1,024 points between 400 and 800 nm at one sample per second using a custom LabVIEW-based program[32].

R scripts described above were used to analyze optical data collected from either $Mb^{-/-}$ or C57BL/6N (WT) hearts. Transmural absorbance data from WT hearts were fit between 535 and 585 nm with reference spectra for hemes b_L and b_H, cytochromes c_1 and cytochrome c and MbO and MbD, together with a line, using a nonlinear least squares regression fitting routine.

The signal-to-noise ratio was calculated by taking the sum of the calculated absorbances of hemes b_L and b_H and cytochromes c_1 and c and dividing this by the sum-squared residuals. If this parameter fell below 100, the data points were excluded from analyses. A total of four data points from three biological replicates were excluded from analyses (Fig. 5e–i).

For one of the nine hearts in Fig. 3k–m, the addition of FCCP was associated with a dramatic increase in absorbance by heme b_H and cytochrome *c*, consistent with hypoxia due to respiratory uncoupling increasing O_2 consumption beyond the amount of O_2 available[33]. This outlier was omitted for the FCCP condition in Fig. 3k–m. This did not affect the statistical significance of the findings.

Langendorff perfused heart studies

To assess cardioactive agents, hearts were perfused for 10 min before sequential administration of 15 µM adenosine, 11.3 mM KCl (final concentration 16 mM) and 2 µM FCCP. Adenosine and KCl were added directly to the buffer, and FCCP was infused at 1% of the coronary flow rate using a syringe pump (Pump 11 Elite, Harvard Apparatus).

To achieve glycogen depletion in the heart, glucose was replaced with 5 mM sodium acetate. Three minutes before ischemia, glucagon (G2044, Sigma-Aldrich) was infused at 10% of the coronary flow rate (final concentration of 2 µg ml^{-1})[66]. To confirm glycogen depletion, the levels of lactate in the heart were measured by LC–MS/MS after 20 min of ischemia. Lactate levels decreased by 66% in hearts perfused with acetate and glucagon. To study mitochondrial inhibitors and uncouplers during ischemia–reperfusion, DMSO stocks of BAM15 or AA5 were diluted in KH buffer and infused at 1% of the coronary flow rate to achieve the desired concentrations. BAM15 (2 µM) was delivered over the first 2.5 min of reperfusion. AA5 (20 nM) was administered 5 min before ischemia, or 200 nm AA5 was administered over the first minute of reperfusion; the higher concentration was required upon reperfusion due to slow uptake.

To assess the impact of substrate availability, hearts were perfused with KH buffer comprising (in mM) 118.4 NaCl, 25 $NaHCO_3$, 4.7 KCl, 1.75 $CaCl_2$, 1.2 $MgSO_4$, 1.2 KH_2PO_4, 5 glucose, 0.2 sodium pyruvate, 1.2 sodium lactate and 0.2 sodium butyrate.

Metabolite analyses

For metabolite assays, hearts were rapidly freeze-clamped using Wollenberger tongs, transferred to precooled Eppendorf tubes and stored at −80 °C. To assess succinate, frozen tissue (10–12 mg) was weighed into a precooled 2-ml, 2.8-mm ceramic Precellys tube (19-628-3, Omni) stored on dry ice. MS extraction buffer (25 µl mg^{-1} tissue) containing 50% (v/v) methanol, 30% (v/v) acetonitrile and 20% (v/v) H_2O and 1 nmol [$^{13}C_4$]succinate internal standard (Sigma-Aldrich) were added to each sample, and samples were rapidly homogenized twice at 6,500 rpm for 15 s using a Precellys 24 tissue homogenizer (Bertin Instruments). Samples were incubated at −20 °C for 1 h and then centrifuged at 17,000*g* for 10 min at 4 °C. The supernatant was centrifuged at 17,000*g* for 10 min at 4 °C and then transferred to a 1.2-ml MS vial (29659, Supelco) on ice and stored at −80 °C. LC–MS/MS was performed using an LCMS-8060 mass spectrometer (Shimadzu) in conjunction with a Nexera X2 UHPLC system (Shimadzu). Samples (5 µl) were injected via a 15-µl flow-through needle, separated at 30 °C by a SeQuant ZIC-HILIC column (3.5 µm, 100 Å, 150 mm × 2.1 mm; Merck Millipore) with a ZIC-HILIC guard column (200 Å, 1 mm × 5 mm) at 200 µl min^{-1}. Buffer A contained 10 mM ammonium bicarbonate, and buffer B contained 100% acetonitrile. A gradient of 80% buffer B was applied between 0 min and 0.1 min, 80–20% buffer B was applied between 0.1 min and 4 min, 20% buffer B was applied between 4 min and 10 min, 20–80% buffer B was applied between 10 min and 11 min and 80% buffer B was applied between 11 min and 15 min to achieve separation. MS was performed in negative ion mode, and multiple-reaction monitoring was used for specific detection of succinate to fragment transitions. Spectra were acquired and analyzed using LabSolutions software (Shimadzu). Compound quantities were calculated against a known concentration of the [$^{13}C_4$]succinate internal standard.

To assess CoQ redox state[53], frozen tissue (3.5–5 mg) was weighed into a precooled 2-ml Precellys tube containing 1.4-mm ceramic beads (19-627-3, Omni) on dry ice and homogenized in 250 µl methanol and 250 µl hexane at 6,500 rpm for 15 s using a Precellys 24 tissue homogenizer (Bertin Instruments), transferred to new tubes and centrifuged at 17,000*g* for 5 min at 4 °C. Then, 20 µl of the upper hexane layer was transferred to a 1.2-ml MS vial (29659, Supelco), and the hexane was evaporated under a stream of N_2 at 37 °C. Dried extracts were resuspended with 2 mM ammonium formate in 1 ml methanol, overlaid with argon and then stored at −20 °C before analysis by LC–MS/MS on the same day. Xevo TQ-S (Waters) was used for LC–MS/MS analyses of CoQ_9 and CoQ_9H_2. Samples were loaded into the autosampler held at 8 °C, and 4 µl of sample was injected via a 15-µl flow-through needle. CoQ_9 and CoQ_9H_2 were separated at 45 °C using an I-Class ACQUITY UPLCr BEH C18 column (2.1 × 50 mm, 130 Å, 1.7 µm; Waters) with a UPLC filter (0.2 µm; Waters). Methanol containing 2 mM ammonium formate was used for the isocratic mobile phase set to a flow rate of 0.8 ml min^{-1}. The mass spectrometer was operated in positive ion mode. MassLynx 4.1 software was used to quantify the peak areas of CoQ_9 and CoQ_9H_2, and the ratio of the peak areas was taken.

Statistics and reproducibility

Data are reported as mean ± s.d. unless otherwise stated. A sample size of at least four biological replicates was used for mitochondrial studies and at least five biological replicates were used for heart studies, consistent with prior reports. Sample sizes for optical studies were validated with a power test for ANOVA using preliminary data. A priori power calculations were performed using the pwr package in R (version 4.4.0). Excluded data are described in the relevant Methods section. The experiments were not randomized, and investigators were not blinded during experiments or analyses. Statistical analyses were performed in GraphPad Prism 9, and statistical tests used are indicated throughout the text and in figure legends. *P* values < 0.05 were considered statistically significant.

Reporting summary

Further information on research design is available in the Nature Portfolio Reporting Summary linked to this article.

Data availability

Source data are provided with this paper.

Code availability

The underlying code for this study is available from Zenodo at https://doi.org/10.5281/zenodo.17465842 (ref. 67).

References

1. Chouchani, E. T. et al. A unifying mechanism for mitochondrial superoxide production during ischemia-reperfusion injury. *CellMetab.* **23**, 254–263 (2016).
2. Nicholls, D. G. & Ferguson, S. J. *Bioenergetics 4* (Academic Press, 2013).
3. Murphy, M. P. & Hartley, R. C. Mitochondria as a therapeutic target for common pathologies. *Nat. Rev. Drug Discov.* https://doi.org/10.1038/nrd.2018.174 (2018).
4. Kobayashi, K. & Neely, J. R. Control of maximum rates of glycolysis in rat cardiac muscle. *Circ. Res.* **44**, 166–175 (1979).
5. Chouchani, E. T. et al. Ischaemic accumulation of succinate controls reperfusion injury through mitochondrial ROS. *Nature* **515**, 431–435 (2014).
6. Lemasters, J. J. et al. Measurement of electrical potential, pH, and free calcium ion concentration in mitochondria of living cells by laser scanning confocal microscopy. *Methods Enzymol.* **260**, 428–444 (1995).
7. Gerencser, A. A. et al. Quantitative measurement of mitochondrial membrane potential in cultured cells: calcium-induced de- and hyperpolarization of neuronal mitochondria. *J. Physiol.* **590**, 2845–2871 (2012).

8. Brand, M. D. in *Bioenergetics: A Practical Approach* (eds Brown, G. C. & Cooper, C.E.) 39–62 (IRL, 1995).
9. Wan, B., Doumen, C., Duszynski, J., Salama, G. & LaNoue, K. F. A method of determining electrical potential gradient across mitochondrial membrane in perfused rat hearts. *Am. J. Physiol.* **265**, H445–H452 (1993).
10. Kauppinen, R. Proton electrochemical potential of the inner mitochondrial membrane in isolated perfused rat hearts, as measured by exogenous probes. *Biochim. Biophys. Acta* **725**, 131–137 (1983).
11. Logan, A. et al. Assessing the mitochondrial membrane potential in cells and in vivo using targeted click chemistry and mass spectrometry. *Cell Metab.* **23**, 379–385 (2016).
12. Kawamoto, A. et al. Measurement of technetium-99m sestamibi signals in rats administered a mitochondrial uncoupler and in a rat model of heart failure. *PLoS ONE* **10**, e0117091 (2015).
13. Alpert, N. M. et al. Quantitative in vivo mapping of myocardial mitochondrial membrane potential. *PLoS ONE* **13**, e0190968 (2018).
14. Andrienko, T., Pasdois, P., Rossbach, A. & Halestrap, A. P. Real-time fluorescence measurements of ROS and [Ca^{2+}] in ischemic/reperfused rat hearts: detectable increases occur only after mitochondrial pore opening and are attenuated by ischemic preconditioning. *PLoS ONE* **11**, e0167300 (2016).
15. Riess, M. L., Camara, A. K., Kevin, L. G., An, J. & Stowe, D. F. Reduced reactive O_2 species formation and preserved mitochondrial NADH and [Ca^{2+}] levels during short-term 17 degrees C ischemia in intact hearts. *J. Mol. Cell. Cardiol.* **61**, 580–590 (2004).
16. Ylitalo, K. V., Ala-Rami, A., Liimatta, E. V., Peuhkurinen, K. J. & Hassinen, I. E. Intracellular free calcium and mitochondrial membrane potential in ischemia/reperfusion and preconditioning. *J. Mol. Cell. Cardiol.* **32**, 1223–1238 (2000).
17. Milliken, A. S., Nadtochiy, S. M. & Brookes, P. S. Inhibiting succinate release worsens cardiac reperfusion injury by enhancing mitochondrial reactive oxygen species generation. *J. Am. Heart Assoc.* **11**, e026135 (2002).
18. Scaduto, R. C. Jr. & Grotyohann, L. W. Measurement of mitochondrial membrane potential using fluorescent rhodamine derivatives. *Biophys. J.* **76**, 469–477 (1999).
19. Porteous, C. M. et al. Rapid uptake of lipophilic triphenylphosphonium cations by mitochondria in vivo following intravenous injection: implications for mitochondria-specific therapies and probes. *Biochim. Biophys. Acta* **1800**, 1009–1017 (2010).
20. Howell, N. & Robertson, D. E. Electrochemical and spectral analysis of the long-range interactions between the Qo and Qi sites and the heme prosthetic groups in ubiquinol-cytochrome *c* oxidoreductase. *Biochemistry* **32**, 11162–11172 (1993).
21. Berry, E. A., Guergova-Kuras, M., Huang, L. S. & Crofts, A. R. Structure and function of cytochrome *bc* complexes. *Annu. Rev. Biochem.* **69**, 1005–1075 (2000).
22. Dutton, P. L., Wilson, D. F. & Lee, C. P. Oxidation-reduction potentials of cytochromes in mitochondria. *Biochemistry* **9**, 5077–5082 (1970).
23. Gopher, A. & Gutman, M. The effect of membrane potential on the redox state of cytochrome b_{561} in antimycin-inhibited submitochondrial particles. *J. Bioenerg. Biomembr.* **12**, 349–367 (1980).
24. Tolkatchev, D., Yu, L. & Yu, C. A. Potential induced redox reactions in mitochondrial and bacterial cytochrome *b*-c_1 complexes. *J. Biol. Chem.* **271**, 12356–12363 (1996).
25. Kim, N., Ripple, M. O. & Springett, R. Measurement of the mitochondrial membrane potential and pH gradient from the redox poise of the hemes of the bc_1 complex. *Biophys. J.* **102**, 1194–1203 (2012).
26. Shinkarev, V. P., Crofts, A. R. & Wraight, C. A. The electric field generated by photosynthetic reaction center induces rapid reversed electron transfer in the bc_1 complex. *Biochemistry* **40**, 12584–12590 (2001).
27. Chance, B. & Williams, G. R. Respiratory enzymes in oxidative phosphorylation. II. Difference spectra. *J. Biol. Chem.* **217**, 395–407 (1955).
28. Keilin, D. & Hardy, W. B. On cytochrome, a respiratory pigment, common to animals, yeast, and higher plants. *Proc. R. Soc. Lond. B* **98**, 312–339 (1925).
29. Tamura, M., Oshino, N., Chance, B. & Silver, I. A. Optical measurements of intracellular oxygen concentration of rat heart in vitro. *Arch. Biochem. Biophys.* **191**, 8–22 (1978).
30. Chess, D. J. et al. Optical spectroscopy in turbid media using an integrating sphere: mitochondrial chromophore analysis during metabolic transitions. *Anal. Biochem.* **439**, 161–172 (2013).
31. Glancy, B., Willis, W. T., Chess, D. J. & Balaban, R. S. Effect of calcium on the oxidative phosphorylation cascade in skeletal muscle mitochondria. *Biochemistry* **52**, 2793–2809 (2013).
32. Femnou, A. N. et al. Intracardiac light catheter for rapid scanning transmural absorbance spectroscopy of perfused myocardium: measurement of myoglobin oxygenation and mitochondria redox state. *Am. J. Physiol.* **313**, H1199–H1208 (2017).
33. Giles, A. V. et al. Paradoxical arteriole constriction compromises cytosolic and mitochondrial oxygen delivery in the isolated saline-perfused heart. *Am. J. Physiol.* **315**, H1791–H1804 (2018).
34. Van Wielink, J. E., Oltmann, L. F., Leeuwerik, F. J., De Hollander, J. A. & Stouthamer, A. H. A method for in situ characterization of *b*- and *c*-type cytochromes in *Escherichia coli* and in complex III from beef heart mitochondria by combined spectrum deconvolution and potentiometric analysis. *Biochim. Biophys. Acta* **681**, 177–190 (1982).
35. Yu, C. A., Yu, L. & King, T. E. Soluble cytochrome *b*-c_1 complex and the reconstitution of succinate-cytochrome c reductase. *J.Biol. Chem.* **249**, 4905–4910 (1974).
36. Bauer, T. M. et al. Perfused murine heart optical transmission spectroscopy using optical catheter and integrating sphere: effects of ischemia/reperfusion. *Anal. Biochem.* **586**, 113443 (2019).
37. Meeson, A. P. et al. Adaptive mechanisms that preserve cardiac function in mice without myoglobin. *Circ. Res.* **88**, 713–720 (2001).
38. Garry, D. J. et al. Mice without myoglobin. *Nature* **395**, 905–908 (1998).
39. Godecke, A. et al. Disruption of myoglobin in mice induces multiple compensatory mechanisms. *Proc. Natl Acad. Sci. USA* **96**, 10495–10500 (1999).
40. Park, J. W., Piknova, B., Dey, S., Noguchi, C. T. & Schechter, A. N. Compensatory mechanisms in myoglobin deficient mice preserve NO homeostasis. *Nitric Oxide* **90**, 10–14 (2019).
41. Guieu, R. et al. Adenosine and the cardiovascular system: the good and the bad. *J. Clin. Med.* https://doi.org/10.3390/jcm9051366 (2020).
42. Pell, V. R. et al. Ischemic preconditioning protects against cardiac ischemia reperfusion injury without affecting succinate accumulation or oxidation. *J. Mol. Cell. Cardiol.* **123**, 88–91 (2018).
43. Hearse, D. J., Garlick, P. B. & Humphrey, S. M. Ischemic contracture of the myocardium: mechanisms and prevention. *Am. J.Cardiol.* **39**, 986–993 (1977).
44. Gruszczyk, A. V. et al. Mitochondrial metabolism and bioenergetic function in an anoxic isolated adult mouse cardiomyocyte model of in vivo cardiac ischemia-reperfusion injury. *Redox Biol.* **54**, 102368 (2022).
45. Grover, G. J. et al. Excessive ATP hydrolysis in ischemic myocardium by mitochondrial F_1F_0-ATPase: effect of selective pharmacological inhibition of mitochondrial ATPase hydrolase activity. *Am. J. Physiol.* **287**, H1747–H1755 (2004).

46. Di Lisa, F. et al. Mitochondrial membrane potential in single living adult rat cardiac myocytes exposed to anoxia or metabolic inhibition. *J. Physiol.* **486**, 1–13 (1995).
47. Martin, J. L. et al. Succinate accumulation drives ischaemia-reperfusion injury during organ transplantation. *Nat. Metab.* **1**, 966–974 (2019).
48. Horn, R. S., Levin, R. & Haugaard, N. The influence of oligomycin on the actions of epinephrine and theophylline upon the perfused rat heart. *Biochem. Pharmacol.* **18**, 503–509 (1969).
49. Prag, H. A. et al. Ischemia-selective cardioprotection by malonate for ischemia/reperfusion injury. *Circ. Res.* **131**, 528–541 (2022).
50. Andrienko, T. N., Pasdois, P., Pereira, G. C., Ovens, M. J. & Halestrap, A. P. The role of succinate and ROS in reperfusion injury—a critical appraisal. *J. Mol. Cell. Cardiol.* **110**, 1–14 (2017).
51. Prag, H. A. et al. Mechanism of succinate efflux upon reperfusion of the ischaemic heart. *Cardiovasc. Res.* **117**, 1188–1201 (2021).
52. Zhang, J. et al. Accumulation of succinate in cardiac ischemia primarily occurs via canonical Krebs cycle activity. *Cell Rep.* **23**, 2617–2628 (2018).
53. Burger, N. et al. A sensitive mass spectrometric assay for mitochondrial CoQ pool redox state in vivo. *Free Radic. Biol. Med.* **147**, 37–47 (2020).
54. James, A. M., Smith, R. A. & Murphy, M. P. Antioxidant and prooxidant properties of mitochondrial coenzyme Q. *Arch. Biochem. Biophys.* **423**, 47–56 (2004).
55. Havens, J. et al. Photoinduced electron transfer in cytochrome bc_1: dynamics of rotation of the iron-sulfur protein during bifurcated electron transfer from ubiquinol to cytochrome c_1 and cytochrome b_L. *Biochim. Biophys. Acta Bioenerg.* **1864**, 148957 (2023).
56. Zhang, J. et al. Oxygen delivery does not limit cardiac performance during high work states. *Am. J. Physiol.* **277**, H50–H57 (1999).
57. Arai, A. E., Kasserra, C. E., Territo, P. R., Gandjbakhche, A. H. & Balaban, R. S. Myocardial oxygenation in vivo: optical spectroscopy of cytoplasmic myoglobin and mitochondrial cytochromes. *Am. J. Physiol.* **277**, H683–H697 (1999).
58. Mootha, V. K., Arai, A. E. & Balaban, R. S. Maximum oxidative phosphorylation capacity of the mammalian heart. *Am. J. Physiol.* **272**, H769–H775 (1997).
59. Glancy, B. et al. Power grid protection of the muscle mitochondrial reticulum. *Cell Rep.* **19**, 487–496 (2017).
60. Wei-LaPierre, L. et al. Respective contribution of mitochondrial superoxide and pH to mitochondria-targeted circularly permuted yellow fluorescent protein (mt-cpYFP) flash activity. *J. Biol. Chem.* **288**, 10567–10577 (2013).
61. Gao, M. et al. Calibration and measurement of mitochondrial pH in intact adult rat cardiomyocytes. *STAR Protoc.* **2**, 100543 (2021).
62. Balaban, R. S., Mootha, V. K. & Arai, A. Spectroscopic determination of cytochrome c oxidase content in tissues containing myoglobin or hemoglobin. *Anal. Biochem.* **237**, 274–278 (1996).
63. Pan, X. et al. The physiological role of mitochondrial calcium revealed by mice lacking the mitochondrial calcium uniporter. *Nat. Cell Biol.* **15**, 1464–1472 (2013).
64. Shinkarev, V. P., Crofts, A. R. & Wraight, C. A. Spectral analysis of the bc_1 complex components in situ: beyond the traditional difference approach. *Biochim. Biophys. Acta* **1757**, 67–77 (2006).
65. Femnou, A. N., Giles, A. & Balaban, R. S. Intra-cardiac side-firing light catheter for monitoring cellular metabolism using transmural absorbance spectroscopy of perfused mammalian hearts. *J. Vis. Exp.* https://doi.org/10.3791/58992 (2019).
66. Vander Heide, R. S., Delyani, J. A., Jennings, R. B., Reimer, K. A. & Steenbergen, C. Reducing lactate accumulation does not attenuate lethal ischemic injury in isolated perfused rat hearts. *Am. J. Physiol.* **270**, H38–H44 (1996).
67. abgiles4. abgiles4/spectral_analysis_mitochondria: spectral analysis in mitochondria. *Zenodo* https://doi.org/10.5281/zenodo.17465842 (2025).

Acknowledgements

R.S.B. was supported by HHS, National Institutes of Health (NIH): ZIA HL004601-35. M.P.M. was supported by the Medical Research Council UK (MC_UU_00028/4) and by a Wellcome Trust investigator award (220257/Z/20/Z). T.K. was supported by the British Heart Foundation (PG/23/11344). E.M. was supported by HHS, National Institutes of Health (NIH): ZO1-HL-002066. We are grateful to L. O. Edwards for technical assistance.

Author contributions

A.V.G.: conceptualization, methodology, ex vivo and in vitro experiments, data analysis and writing. R.C.: methodology and data analysis. H.A.P.: LC–MS/MS, data analysis and writing. N.B.: LC–MS/MS, methodology and data analysis. B.L.: methodology and data analysis. C.S.Y.: methodology, LC–MS/MS and data analysis. J.S.: methodology and in vitro experiments. E.M.: conceptualization, methodology, supervision and writing. T.K.: conceptualization, funding acquisition, supervision and writing. M.P.M.: conceptualization, funding acquisition, supervision and writing. R.S.B.: conceptualization, funding acquisition, supervision and writing.

Competing interests

T.K. and M.P.M. are founders and officers of Camoxis Pharmaceuticals. The other authors declare no competing interests.

Additional information

Extended data is available for this paper at https://doi.org/10.1038/s44161-025-00752-9.

Supplementary information The online version contains supplementary material available at https://doi.org/10.1038/s44161-025-00752-9.

Correspondence and requests for materials should be addressed to Michael P. Murphy or Robert S. Balaban.

Peer review information *Nature Cardiovascular Research* thanks Andrew Halestrap and the other, anonymous, reviewer(s) for their contribution to the peer review of this work.

https://doi.org/10.1038/s44161-025-00752-9

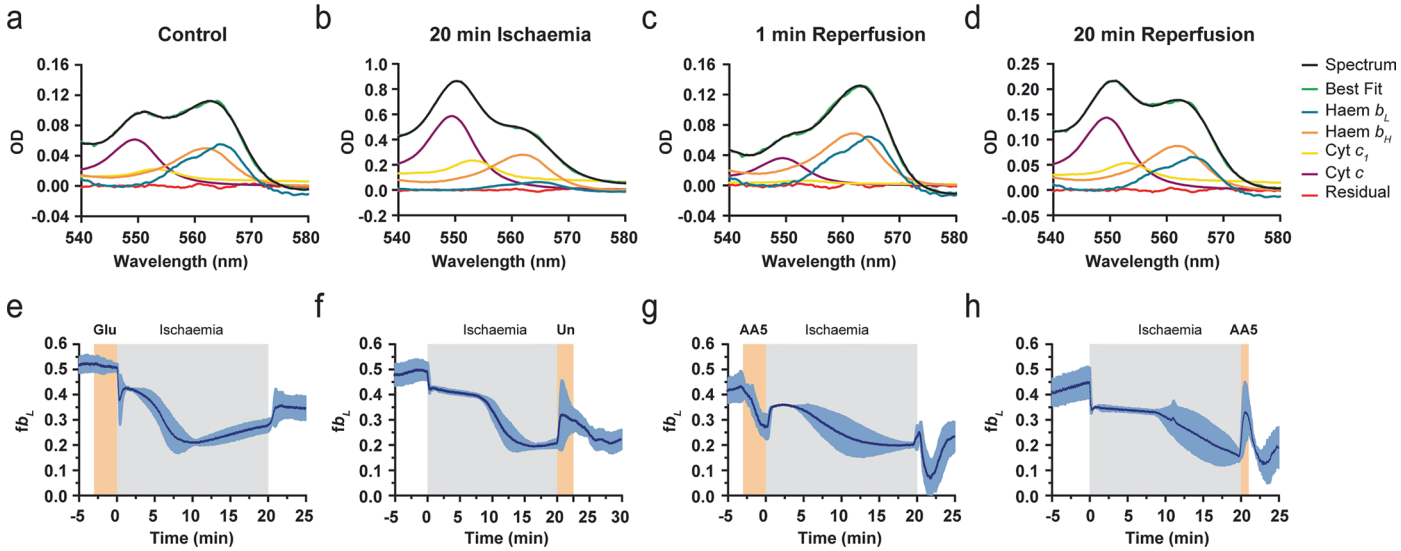

Extended Data Fig. 1 | Measurement of ΔΨm in the Mb$^{-/-}$ heart during IR injury. a–d, The isolated perfused Mb$^{-/-}$ heart was subjected to global ischemia-reperfusion, and a multi-wavelength nonlinear least squares regression was performed on the experimental spectra collected under normoxic conditions (**a**), after 20 min of ischemia (**b**) and at 1 (**c**) and 20 (**d**) minutes of reperfusion using reference spectra for mitochondrial cytochromes and a line. After spectral fitting, the linear component was subtracted from all experimental spectra and best fits. **e**, Isolated perfused Mb$^{-/-}$ hearts were perfused with glucose-free KH buffer supplemented with sodium acetate and administered glucagon (indicated by Glu) 3 min prior to ischemia ($n = 5$). Transmural absorbance was measured every second, and a rolling average of five consecutive spectra was taken prior to multi-wavelength nonlinear least squares regression analysis. Heme b_L and b_H absorbances were quantified, and fb_L was calculated over time. **f–h**, Isolated perfused Mb$^{-/-}$ hearts received 2 μM BAM ($n = 5$) (indicated by Un) (**f**) at the onset of reperfusion or 20 nM AA5 ($n = 5$) (indicated by AA5) (**g**) 3 min prior to 20 min of global ischemia or 200 nM ($n = 5$) (indicated by AA5) (**h**) at the onset of reperfusion. fb_L was calculated over time as described above. All data are means ± s.d.

https://doi.org/10.1038/s44161-025-00752-9

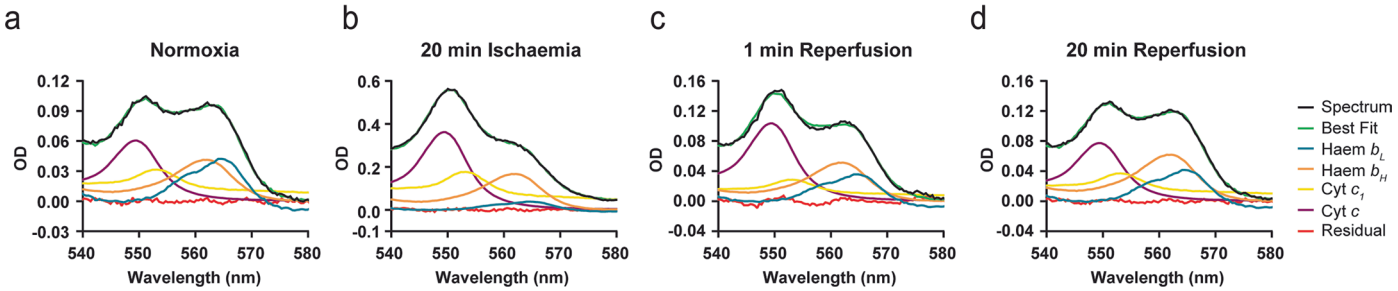

Extended Data Fig. 2 | Multi-wavelength absorbance spectroscopy in the isolated Wt heart. a–d, Isolated perfused Wt mouse hearts ($n = 9$) were subjected to global ischemia-reperfusion, and a multi-wavelength nonlinear least squares regression was performed on experimental spectra collected under normoxic conditions (**a**), after 20 min of ischemia (**b**) and at 1 (**c**) and 20 (**d**) minutes of reperfusion. After spectral fitting, MbO, MbD and the linear component were subtracted from all experimental spectra and best fits.

nature portfolio

Corresponding author(s): Michael P Murphy

Last updated by author(s): Oct 27, 2025

Reporting Summary

Nature Portfolio wishes to improve the reproducibility of the work that we publish. This form provides structure for consistency and transparency in reporting. For further information on Nature Portfolio policies, see our Editorial Policies and the Editorial Policy Checklist.

Statistics

For all statistical analyses, confirm that the following items are present in the figure legend, table legend, main text, or Methods section.

n/a	Confirmed	
☐	☒	The exact sample size (*n*) for each experimental group/condition, given as a discrete number and unit of measurement
☐	☒	A statement on whether measurements were taken from distinct samples or whether the same sample was measured repeatedly
☐	☒	The statistical test(s) used AND whether they are one- or two-sided *Only common tests should be described solely by name; describe more complex techniques in the Methods section.*
☐	☒	A description of all covariates tested
☐	☒	A description of any assumptions or corrections, such as tests of normality and adjustment for multiple comparisons
☐	☒	A full description of the statistical parameters including central tendency (e.g. means) or other basic estimates (e.g. regression coefficient) AND variation (e.g. standard deviation) or associated estimates of uncertainty (e.g. confidence intervals)
☐	☒	For null hypothesis testing, the test statistic (e.g. *F*, *t*, *r*) with confidence intervals, effect sizes, degrees of freedom and *P* value noted *Give P values as exact values whenever suitable.*
☐	☒	For Bayesian analysis, information on the choice of priors and Markov chain Monte Carlo settings
☐	☒	For hierarchical and complex designs, identification of the appropriate level for tests and full reporting of outcomes
☐	☒	Estimates of effect sizes (e.g. Cohen's *d*, Pearson's *r*), indicating how they were calculated

Our web collection on statistics for biologists contains articles on many of the points above.

Software and code

Policy information about availability of computer code

Data collection	Cardiac functional data were collected and analyzed using the ADInstruments PowerLab data acquisition system in conjunction with LabChart 8 software. Optical data were acquired using a custom LabVIEW program, as described in a previously published protocol.
Data analysis	Analysis of optical data was performed using custom scripts written in R. (version 4.4.0). The freely available packages minpack.lm, ggplot2, zoo, and pwr were used in these analyses. The underlying code for this study is available from the corresponding author(s) upon request.

For manuscripts utilizing custom algorithms or software that are central to the research but not yet described in published literature, software must be made available to editors and reviewers. We strongly encourage code deposition in a community repository (e.g. GitHub). See the Nature Portfolio guidelines for submitting code & software for further information.

Data

Policy information about availability of data

All manuscripts must include a data availability statement. This statement should provide the following information, where applicable:

- Accession codes, unique identifiers, or web links for publicly available datasets
- A description of any restrictions on data availability
- For clinical datasets or third party data, please ensure that the statement adheres to our policy

Source data are provided with this paper. All data supporting the findings of the study are available from the corresponding author(s) upon request.

Research involving human participants, their data, or biological material

Policy information about studies with human participants or human data. See also policy information about sex, gender (identity/presentation), and sexual orientation and race, ethnicity and racism.

Reporting on sex and gender	*Use the terms sex (biological attribute) and gender (shaped by social and cultural circumstances) carefully in order to avoid confusing both terms. Indicate if findings apply to only one sex or gender; describe whether sex and gender were considered in study design; whether sex and/or gender was determined based on self-reporting or assigned and methods used.* *Provide in the source data disaggregated sex and gender data, where this information has been collected, and if consent has been obtained for sharing of individual-level data; provide overall numbers in this Reporting Summary. Please state if this information has not been collected.* *Report sex- and gender-based analyses where performed, justify reasons for lack of sex- and gender-based analysis.*
Reporting on race, ethnicity, or other socially relevant groupings	*Please specify the socially constructed or socially relevant categorization variable(s) used in your manuscript and explain why they were used. Please note that such variables should not be used as proxies for other socially constructed/relevant variables (for example, race or ethnicity should not be used as a proxy for socioeconomic status).* *Provide clear definitions of the relevant terms used, how they were provided (by the participants/respondents, the researchers, or third parties), and the method(s) used to classify people into the different categories (e.g. self-report, census or administrative data, social media data, etc.)* *Please provide details about how you controlled for confounding variables in your analyses.*
Population characteristics	*Describe the covariate-relevant population characteristics of the human research participants (e.g. age, genotypic information, past and current diagnosis and treatment categories). If you filled out the behavioural & social sciences study design questions and have nothing to add here, write "See above."*
Recruitment	*Describe how participants were recruited. Outline any potential self-selection bias or other biases that may be present and how these are likely to impact results.*
Ethics oversight	*Identify the organization(s) that approved the study protocol.*

Note that full information on the approval of the study protocol must also be provided in the manuscript.

Field-specific reporting

Please select the one below that is the best fit for your research. If you are not sure, read the appropriate sections before making your selection.

☒ Life sciences ☐ Behavioural & social sciences ☐ Ecological, evolutionary & environmental sciences

For a reference copy of the document with all sections, see nature.com/documents/nr-reporting-summary-flat.pdf

Life sciences study design

All studies must disclose on these points even when the disclosure is negative.

Sample size	A sample size of at least 4 biological replicates was used for all mitochondria studies. In all but one isolated heart study, a sample size of at least 6 was used for statistical comparisons. Samples sizes for optical studies of the heart were determined using a power test for ANOVA using preliminary data. A priori power calculations were performed using the pwr package in R (version 4.4.0).
Data exclusions	For 1 of the 9 hearts in Fig. 3k-m the addition of FCCP was associated with a dramatic increase in absorbance by haem bH and cytochrome c, consistent with hypoxia due to respiratory uncoupling increasing O2 consumption beyond that available. This outlier was omitted for the FCCP condition in Fig. 3k-m. This did not affect the statistical significance of the findings. This description is included in the Methods. Furthermore, in Wt animals, a signal to noise threshold was established leading to the exclusion of selected data points in Fig. 5e-i. The signal to noise ratio was calculated by taking the sum of the calculated absorbances of cytochrome bL, bH, c1, and c and dividing this by the sum squared residuals. If this parameter fell below 100 then these data points were excluded from analyses. A total of 4 data points from 3 biological replicates were excluded from analyses (Fig. 5e-i). Data exclusions are described in the relevant Methods sections.
Replication	Consistent protocols were used across all experimental groups and studies to ensure reproducibility. When possible, experimental groups were assessed in close succession (e.g., same day or week) or at the same time (e.g., mass spectrometry) with the same reagents or buffer stocks. All compounds used were from the same lot and were stored in aliquots to avoid freeze thaw. Furthermore, biological replicates were collected for all studies and litter mates used when possible and where appropriate.
Randomization	When possible, litter mates were used and separated into treatment groups (e.g., glucose-only or complex buffer) randomly.
Blinding	Blinding was not employed due to the nature of the experimental design and analyses (e.g., Wt versus myoglobin knockout are visibly distinct phenotypes requiring distinct analyses approaches). However, data analysis was performed using objective, quantitative measures that obviated the need for blinding. Consistent protocols were used across all experimental groups to ensure reproducibility.

Behavioural & social sciences study design

All studies must disclose on these points even when the disclosure is negative.

Study description	*Briefly describe the study type including whether data are quantitative, qualitative, or mixed-methods (e.g. qualitative cross-sectional, quantitative experimental, mixed-methods case study).*
Research sample	*State the research sample (e.g. Harvard university undergraduates, villagers in rural India) and provide relevant demographic information (e.g. age, sex) and indicate whether the sample is representative. Provide a rationale for the study sample chosen. For studies involving existing datasets, please describe the dataset and source.*
Sampling strategy	*Describe the sampling procedure (e.g. random, snowball, stratified, convenience). Describe the statistical methods that were used to predetermine sample size OR if no sample-size calculation was performed, describe how sample sizes were chosen and provide a rationale for why these sample sizes are sufficient. For qualitative data, please indicate whether data saturation was considered, and what criteria were used to decide that no further sampling was needed.*
Data collection	*Provide details about the data collection procedure, including the instruments or devices used to record the data (e.g. pen and paper, computer, eye tracker, video or audio equipment) whether anyone was present besides the participant(s) and the researcher, and whether the researcher was blind to experimental condition and/or the study hypothesis during data collection.*
Timing	*Indicate the start and stop dates of data collection. If there is a gap between collection periods, state the dates for each sample cohort.*
Data exclusions	*If no data were excluded from the analyses, state so OR if data were excluded, provide the exact number of exclusions and the rationale behind them, indicating whether exclusion criteria were pre-established.*
Non-participation	*State how many participants dropped out/declined participation and the reason(s) given OR provide response rate OR state that no participants dropped out/declined participation.*
Randomization	*If participants were not allocated into experimental groups, state so OR describe how participants were allocated to groups, and if allocation was not random, describe how covariates were controlled.*

Ecological, evolutionary & environmental sciences study design

All studies must disclose on these points even when the disclosure is negative.

Study description	*Briefly describe the study. For quantitative data include treatment factors and interactions, design structure (e.g. factorial, nested, hierarchical), nature and number of experimental units and replicates.*
Research sample	*Describe the research sample (e.g. a group of tagged Passer domesticus, all Stenocereus thurberi within Organ Pipe Cactus National Monument), and provide a rationale for the sample choice. When relevant, describe the organism taxa, source, sex, age range and any manipulations. State what population the sample is meant to represent when applicable. For studies involving existing datasets, describe the data and its source.*
Sampling strategy	*Note the sampling procedure. Describe the statistical methods that were used to predetermine sample size OR if no sample-size calculation was performed, describe how sample sizes were chosen and provide a rationale for why these sample sizes are sufficient.*
Data collection	*Describe the data collection procedure, including who recorded the data and how.*
Timing and spatial scale	*Indicate the start and stop dates of data collection, noting the frequency and periodicity of sampling and providing a rationale for these choices. If there is a gap between collection periods, state the dates for each sample cohort. Specify the spatial scale from which the data are taken*
Data exclusions	*If no data were excluded from the analyses, state so OR if data were excluded, describe the exclusions and the rationale behind them, indicating whether exclusion criteria were pre-established.*
Reproducibility	*Describe the measures taken to verify the reproducibility of experimental findings. For each experiment, note whether any attempts to repeat the experiment failed OR state that all attempts to repeat the experiment were successful.*
Randomization	*Describe how samples/organisms/participants were allocated into groups. If allocation was not random, describe how covariates were controlled. If this is not relevant to your study, explain why.*
Blinding	*Describe the extent of blinding used during data acquisition and analysis. If blinding was not possible, describe why OR explain why blinding was not relevant to your study.*

Did the study involve field work? ☐ Yes ☐ No

Field work, collection and transport

Field conditions	*Describe the study conditions for field work, providing relevant parameters (e.g. temperature, rainfall).*
Location	*State the location of the sampling or experiment, providing relevant parameters (e.g. latitude and longitude, elevation, water depth).*
Access & import/export	*Describe the efforts you have made to access habitats and to collect and import/export your samples in a responsible manner and in compliance with local, national and international laws, noting any permits that were obtained (give the name of the issuing authority, the date of issue, and any identifying information).*
Disturbance	*Describe any disturbance caused by the study and how it was minimized.*

Reporting for specific materials, systems and methods

We require information from authors about some types of materials, experimental systems and methods used in many studies. Here, indicate whether each material, system or method listed is relevant to your study. If you are not sure if a list item applies to your research, read the appropriate section before selecting a response.

Materials & experimental systems

n/a	Involved in the study
☒	☐ Antibodies
☒	☐ Eukaryotic cell lines
☒	☐ Palaeontology and archaeology
☐	☒ Animals and other organisms
☒	☐ Clinical data
☒	☐ Dual use research of concern
☒	☐ Plants

Methods

n/a	Involved in the study
☒	☐ ChIP-seq
☒	☐ Flow cytometry
☒	☐ MRI-based neuroimaging

Antibodies

Antibodies used	N/A
Validation	N/A

Eukaryotic cell lines

Policy information about cell lines and Sex and Gender in Research

Cell line source(s)	N/A
Authentication	N/A
Mycoplasma contamination	N/A
Commonly misidentified lines (See ICLAC register)	N/A

Palaeontology and Archaeology

Specimen provenance	*Provide provenance information for specimens and describe permits that were obtained for the work (including the name of the issuing authority, the date of issue, and any identifying information). Permits should encompass collection and, where applicable, export.*
Specimen deposition	*Indicate where the specimens have been deposited to permit free access by other researchers.*
Dating methods	*If new dates are provided, describe how they were obtained (e.g. collection, storage, sample pretreatment and measurement), where they were obtained (i.e. lab name), the calibration program and the protocol for quality assurance OR state that no new dates are provided.*

☐ Tick this box to confirm that the raw and calibrated dates are available in the paper or in Supplementary Information.

Ethics oversight	*Identify the organization(s) that approved or provided guidance on the study protocol, OR state that no ethical approval or guidance was required and explain why not.*

Note that full information on the approval of the study protocol must also be provided in the manuscript.

Animals and other research organisms

Policy information about studies involving animals; ARRIVE guidelines recommended for reporting animal research, and Sex and Gender in Research

Laboratory animals	Mice: Male and female C57Bl6N (9-16 weeks) from Taconic (Rensselaer, NY) or Mb-/- mice (9-16 weeks) maintained in NIH facilities. Rabbits: Male New Zealand White rabbits from Charles River (6 mo-1 yr, 3-5 kg).
Wild animals	None.
Reporting on sex	Male rabbits were used exclusively for isolated rabbit heart mitochondria studies, while both male and female mice were used in isolated mouse mitochondria and heart studies. Data were not disaggregated by sex because the experimental question did not involve sex-specific differences and was not directly related to clinical translation in which sex as a variable must be considered. While there was no clear sex-based variability, the study was not powered appropriately to detect sex differences. For this reason, data from both sexes were pooled to address the primary research goal which focused on the development of a technique for measuring mitochondrial membrane potential that could be readily applied to biological systems regardless of sex. Future studies designed specifically to evaluate sex as a biological variable are warranted.
Field-collected samples	None.
Ethics oversight	All animal protocols were approved by the National Heart, Lung, and Blood Institute Animal Care and Use Committee and experiments with rabbits and mice were performed in accordance with the guidelines described in the Animal Welfare Act (AWA).

Note that full information on the approval of the study protocol must also be provided in the manuscript.

Clinical data

Policy information about clinical studies

All manuscripts should comply with the ICMJE guidelines for publication of clinical research and a completed CONSORT checklist must be included with all submissions.

Clinical trial registration	N/A
Study protocol	N/A
Data collection	N/A
Outcomes	N/A

Dual use research of concern

Policy information about dual use research of concern

Hazards

Could the accidental, deliberate or reckless misuse of agents or technologies generated in the work, or the application of information presented in the manuscript, pose a threat to:

No	Yes	
☒	☐	Public health
☒	☐	National security
☒	☐	Crops and/or livestock
☒	☐	Ecosystems
☒	☐	Any other significant area

Experiments of concern

Does the work involve any of these experiments of concern:

No	Yes	
☒	☐	Demonstrate how to render a vaccine ineffective
☒	☐	Confer resistance to therapeutically useful antibiotics or antiviral agents
☒	☐	Enhance the virulence of a pathogen or render a nonpathogen virulent
☒	☐	Increase transmissibility of a pathogen
☒	☐	Alter the host range of a pathogen
☒	☐	Enable evasion of diagnostic/detection modalities
☒	☐	Enable the weaponization of a biological agent or toxin
☒	☐	Any other potentially harmful combination of experiments and agents

Plants

Seed stocks	N/A
Novel plant genotypes	N/A
Authentication	N/A

ChIP-seq

Data deposition

☐ Confirm that both raw and final processed data have been deposited in a public database such as GEO.

☐ Confirm that you have deposited or provided access to graph files (e.g. BED files) for the called peaks.

Data access links *May remain private before publication.*	*For "Initial submission" or "Revised version" documents, provide reviewer access links. For your "Final submission" document, provide a link to the deposited data.*
Files in database submission	*Provide a list of all files available in the database submission.*
Genome browser session (e.g. UCSC)	*Provide a link to an anonymized genome browser session for "Initial submission" and "Revised version" documents only, to enable peer review. Write "no longer applicable" for "Final submission" documents.*

Methodology

Replicates	*Describe the experimental replicates, specifying number, type and replicate agreement.*
Sequencing depth	*Describe the sequencing depth for each experiment, providing the total number of reads, uniquely mapped reads, length of reads and whether they were paired- or single-end.*
Antibodies	*Describe the antibodies used for the ChIP-seq experiments; as applicable, provide supplier name, catalog number, clone name, and lot number.*
Peak calling parameters	*Specify the command line program and parameters used for read mapping and peak calling, including the ChIP, control and index files used.*
Data quality	*Describe the methods used to ensure data quality in full detail, including how many peaks are at FDR 5% and above 5-fold enrichment.*
Software	*Describe the software used to collect and analyze the ChIP-seq data. For custom code that has been deposited into a community repository, provide accession details.*

Flow Cytometry

Plots

Confirm that:

☐ The axis labels state the marker and fluorochrome used (e.g. CD4-FITC).

☐ The axis scales are clearly visible. Include numbers along axes only for bottom left plot of group (a 'group' is an analysis of identical markers).

☐ All plots are contour plots with outliers or pseudocolor plots.

☐ A numerical value for number of cells or percentage (with statistics) is provided.

Methodology

Sample preparation	*Describe the sample preparation, detailing the biological source of the cells and any tissue processing steps used.*
Instrument	*Identify the instrument used for data collection, specifying make and model number.*
Software	*Describe the software used to collect and analyze the flow cytometry data. For custom code that has been deposited into a community repository, provide accession details.*
Cell population abundance	*Describe the abundance of the relevant cell populations within post-sort fractions, providing details on the purity of the samples and how it was determined.*
Gating strategy	*Describe the gating strategy used for all relevant experiments, specifying the preliminary FSC/SSC gates of the starting cell population, indicating where boundaries between "positive" and "negative" staining cell populations are defined.*

☐ Tick this box to confirm that a figure exemplifying the gating strategy is provided in the Supplementary Information.

Magnetic resonance imaging

Experimental design

Design type	*Indicate task or resting state; event-related or block design.*
Design specifications	*Specify the number of blocks, trials or experimental units per session and/or subject, and specify the length of each trial or block (if trials are blocked) and interval between trials.*
Behavioral performance measures	*State number and/or type of variables recorded (e.g. correct button press, response time) and what statistics were used to establish that the subjects were performing the task as expected (e.g. mean, range, and/or standard deviation across subjects).*

Acquisition

Imaging type(s)	*Specify: functional, structural, diffusion, perfusion.*
Field strength	*Specify in Tesla*
Sequence & imaging parameters	*Specify the pulse sequence type (gradient echo, spin echo, etc.), imaging type (EPI, spiral, etc.), field of view, matrix size, slice thickness, orientation and TE/TR/flip angle.*
Area of acquisition	*State whether a whole brain scan was used OR define the area of acquisition, describing how the region was determined.*

Diffusion MRI ☐ Used ☐ Not used

Preprocessing

Preprocessing software	*Provide detail on software version and revision number and on specific parameters (model/functions, brain extraction, segmentation, smoothing kernel size, etc.).*
Normalization	*If data were normalized/standardized, describe the approach(es): specify linear or non-linear and define image types used for transformation OR indicate that data were not normalized and explain rationale for lack of normalization.*
Normalization template	*Describe the template used for normalization/transformation, specifying subject space or group standardized space (e.g. original Talairach, MNI305, ICBM152) OR indicate that the data were not normalized.*
Noise and artifact removal	*Describe your procedure(s) for artifact and structured noise removal, specifying motion parameters, tissue signals and physiological signals (heart rate, respiration).*

Volume censoring

Define your software and/or method and criteria for volume censoring, and state the extent of such censoring.

Statistical modeling & inference

Model type and settings

Specify type (mass univariate, multivariate, RSA, predictive, etc.) and describe essential details of the model at the first and second levels (e.g. fixed, random or mixed effects; drift or auto-correlation).

Effect(s) tested

Define precise effect in terms of the task or stimulus conditions instead of psychological concepts and indicate whether ANOVA or factorial designs were used.

Specify type of analysis: ☐ Whole brain ☐ ROI-based ☐ Both

Statistic type for inference

Specify voxel-wise or cluster-wise and report all relevant parameters for cluster-wise methods.

(See Eklund et al. 2016)

Correction

Describe the type of correction and how it is obtained for multiple comparisons (e.g. FWE, FDR, permutation or Monte Carlo).

Models & analysis

n/a	Involved in the study
☐	☐ Functional and/or effective connectivity
☐	☐ Graph analysis
☐	☐ Multivariate modeling or predictive analysis

Functional and/or effective connectivity

Report the measures of dependence used and the model details (e.g. Pearson correlation, partial correlation, mutual information).

Graph analysis

Report the dependent variable and connectivity measure, specifying weighted graph or binarized graph, subject- or group-level, and the global and/or node summaries used (e.g. clustering coefficient, efficiency, etc.).

Multivariate modeling and predictive analysis

Specify independent variables, features extraction and dimension reduction, model, training and evaluation metrics.